NUREG/CR-1499
ORNL/NUREG/CSD/TM-14
Distribution Category RF

TWO FINITE ELEMENT TECHNIQUES FOR COMPUTING MODE I STRESS INTENSITY FACTORS IN TWO- OR THREE-DIMENSIONAL PROBLEMS

S. K. Iskander

Sponsor: R. D. Cheverton

Manuscript Completed: November 1979

Date Published: February 1981

Prepared for the
Office of Nuclear Regulatory Research
U. S. Nuclear Regulatory Commission
Washington, DC 20555
Under Interagency Agreements DOE 40-551-75 and 40-552-75

NRC FIN No. B0119

COMPUTER SCIENCES DIVISION
at
Oak Ridge Gaseous Diffusion Plant
Post Office Box P
Oak Ridge, Tennessee 37830

Union Carbide Corporation, Nuclear Division
operating the
Oak Ridge Gaseous Diffusion Plant . Oak Ridge National Laboratory
Oak Ridge Y-12 Plant . Paducah Gaseous Diffusion Plant
under Contract No. W-7405-eng-26
for the
Department of Energy

TABLE OF CONTENTS

TABLE OF CONTENTS (Contd.)

FOREWORD

The work reported here was performed at Oak Ridge National Laboratory (ORNL) under sponsorship of the U.S. Nuclear Regulatory Commission's (NRC's) Heavy-Section Steel Technology Program, which is directed by ORNL. The program is conducted as part of the ORNL Pressure Vessel Technology Program, of which G. D. Whitman is manager. The manager for the NRC is Milton Vagins.

This report is designated Heavy-Section Steel Technology Program Technical Report 58. Prior reports in this series are listed below:

1. S. Yukawa, *Evaluation of Periodic Proof Testing and Warm Prestressing Procedures for Nuclear Reactor Vessels,* HSSTP-TR-1, General Electric Company, Schenectady, N.Y. (July 1, 1969).
2. L. W. Loechel, *The Effect of Section Size on the Transition Temperature in Steel,* MCR-69-189, Martin Marietta Corporation, Denver, Colo. (Nov. 20, 1969).
3. P. N. Randall, *Gross Strain Measure of Fracture Toughness of Steels,* HSSTP-TR-3, TRW Systems Group, Redondo Beach, Calif. (Nov. 1, 1969).
4. C. Visser, S. E. Gabrielse, and W. VanBuren, *A Two-Dimensional Elastic-Plastic Analysis of Fracture Test Specimens,* WCAP-7368, Westinghouse Electric Corporation, PWR Systems Division, Pittsburgh, Pa. (October 1969).
5. T. R. Mager, F. O. Thomas, and W. S. Hazelton, *Evaluation by Linear Elastic Fracture Mechanics of Radiation Damage to Pressure Vessel Steels,* WCAP-7328 (Rev.), Westinghouse Electric Corporation, PWR Systems Division, Pittsburgh, Pa. (October 1969).
6. W. O. Shabbits, W. H. Pryle, and E. T. Wessel, *Heavy Section Fracture Toughness Properties of A533 Grade B Class 1 Steel Plate and Submerged Arc Weldment,* WCAP-7414, Westinghouse Electric Corporation, PWR Systems Division, Pittsburgh, Pa. (December 1969).
7. F. J. Loss, *Dynamic Tear Test Investigations of the Fracture Toughness of Thick-Section Steel,* NRL-7056, U.S. Naval Research Laboratory, Washington, D.C. (May 14, 1970).
8. P. B. Crosley and E. J. Ripling, *Crack Arrest Fracture Toughness of A533 Grade B Class 1 Pressure Vessel Steel,* HSSTP-TR-8, Materials Research Laboratory, Inc., Glenwood, Ill. (March 1970).
9. T. R. Mager, *Post-Irradiation Testing of 2T Compact Tension Specimens,* WCAP-7561, Westinghouse Electric Corporation, PWR Systems Division, Pittsburgh, Pa. (August 1970).
10. T. R. Mager, *Fracture Toughness Characterization Study of A533, Grade B, Class 1 Steel,* WCAP-7578, Westinghouse Electric Corporation, PWR Systems Division, Pittsburgh, Pa. (October 1970).
11. T. R. Mager, *Notch Preparation in Compact Tension Specimens,* WCAP-7579, Westinghouse Electric Corporation, PWR Systems Division, Pittsburgh, Pa. (November 1970).
12. N. Levy and P. V. Marcal, *Three-Dimensional Elastic-Plastic Stress and Strain Analysis for Fracture Mechanics, Phase I: Simple Flawed Specimens,* HSSTP-TR-12, Brown University, Providence, R.I. (December 1970).
13. W. O. Shabbits, *Dynamic Fracture Toughness Properties of Heavy Section A533 Grade B, Class 1 Steel Plate,* WCAP-7623, Westinghouse Electric Corporation, PWR Systems Division, Pittsburgh, Pa. (December 1970).
14. P. N. Randall, *Gross Strain Crack Tolerance of A533-B Steel,* HSSTP-TR-14, TRW Systems Group, Redondo Beach, Calif. (May 1, 1971).

15. H. T. Corten and R. H. Sailors, *Relationship Between Material Fracture Toughness Using Fracture Mechanics and Transition Temperature Tests*, T&AM Report 346, University of Illinois, Urbana, Ill. (Aug. 1, 1971).
16. T. R. Mager and V. J. McLoughlin, *The Effect of an Environment of High Temperature Primary Grade Nuclear Reactor Water on the Fatigue Crack Growth Characteristics of A533 Grade B Class 1 Plate and Weldment Material*, WCAP-7776, Westinghouse Electric Corporation, PWR Systems Division, Pittsburgh, Pa. (October 1971).
17. N. Levy and P. V. Marcal, *Three-Dimensional Elastic-Plastic Stress and Strain Analysis for Fracture Mechanics, Phase II: Improved Modeling*, HSSTP-TR-17, Brown University, Providence, R.I. (November 1971).
18. S. C. Grigory, *Six-inch-thick Flawed Tensile Tests, First Technical Summary Report, Longitudinal Specimens 1 through 7*, HSSTP-TR-18, Southwest Research Institute, San Antonio, Tex. (June 1972).
19. P. N. Randall, *Effects of Strain Gradients on the Gross Strain Crack Tolerance of A533-B Steel*, HSSTP-TR-19, TRW Systems Group, Redondo Beach, Calif. (May 1, 1972).
20. S. C. Grigory, *Tests of Six-inch-thick Flawed Tensile Specimens, Second Technical Summary Report, Transverse Specimens Numbers 8 through 10, Welded Specimens Numbers 11 through 13*, HSSTP-TR-20, Southwest Research Institute, San Antonio, Tex. (June 1972).
21. L. A. James and J. A. Williams, *Heavy-Section Steel Technology Program Technical Report No. 21, The Effect of Temperature and Neutron Irradiation upon the Fatigue-Crack Propagation Behavior of ASTM A533, Grade B, Class 1 Steel*, HEDL-TME-72-132, Hanford Engineering Development Laboratory, Richland, Wash. (September 1972).
22. S. C. Grigory, *Tests of Six-inch-thick Flawed Tensile Specimens, Third Technical Summary Report, Longitudinal Specimens Numbers 14 through 16, Unflawed Specimen Number 17*, HSSTP-TR-22, Southwest Research Institute, San Antonio, Tex. (October 1972).
23. S. C. Grigory, *Tests of Six-inch-thick Flawed Tensile Specimens, Fourth Technical Summary Report, Tests of One-inch-thick Flawed Tensile Specimens for Size Effect Evaluation*, HSSTP-TR-23, Southwest Research Institute, San Antonio, Tex. (June 1973).
24. S. P. Ying and S. C. Grigory, *Tests of Six-inch-thick Tensile Specimens, Fifth Technical Summary Report, Acoustic Emission Monitoring of One-inch and Six-inch-thick Tensile Specimens*, HSSTP-TR-24, Southwest Research Institute, San Antonio, Tex. (November 1972).
25. R. W. Derby et al., *Test of 6-inch-thick Pressure Vessels, Series 1: Intermediate Test Vessels V-1 and V-2*, ORNL-4895 (February 1974).
26. W. J. Stelzman and R. G. Berggren, *Radiation Strengthening and Embrittlement in Heavy Section Plates and Welds*, ORNL-4871 (June 1973).
27. P. B. Crosley and E. J. Ripling, *Crack Arrest in an Increas[illegible]eld*, HSSTP-TR-27, Materials Research Laboratory, Glenwood, Ill. (January 1973).
28. P. V. Marcal, P. M. Stuart, and R. S. Bettes, *Elastic-Plastic Behavior of a Longitudinal Semi-Elliptical Crack in a Thick Pressure Vessel*, Brown University, Providence, R.I. (June 1973).
29. W. J. Stelzman, *Characterization of HSST Plates 01, 02, and 03* (in preparation).
30. D. A. Canonico, *Characterization of Heavy Section Weldments in Pressure Vessel Steels* (in preparation).
31. J. A. Williams, *The Irradiation and Temperature Dependence of Tensile and Fracture Properties of ASTM A533, Grade B, Class 1 Steel Plate and Weldment*, HEDL-TME 73—75, Hanford Engineering Development Laboratory, Richland, Wash. (August 1973).

32. J. M. Steichen and J. A. Williams, *High Strain Rate Tensile Properties of Irradiated ASTM A533 Grade B Class 1 Pressure Vessel Steel*, HEDL-TME 73-74, Hanford Engineering Development Laboratory, Richland, Wash. (July 1973).
33. P. C. Riccardella and J. L. Swedlow, *A Combined Analytical-Experimental Fracture Study*, WCAP-8224, Westinghouse Electric Corporation, PWR Systems Division, Pittsburgh, Pa. (October 1973).
34. R. J. Podlasek and R. J. Eiber, *Final Report on Investigation of Mode III Crack Extension in Reactor Piping*, Battelle Laboratories, Columbus, Ohio (May 1974).
35. T. R. Mager et al., *Interim Report on the Effect of Low Frequencies on the Fatigue Crack Growth Characteristics of A533 Grade B Class 1 Plate in an Environment of High-Temperature Primary Grade Nuclear Reactor Water*, WCAP-8256, Westinghouse Electric Corporation, Pittsburgh, Pa. (December 1973).
36. J. A. Williams, *The Irradiated Fracture Toughness of ASTM A533, Grade B, Class 1 Steel Measured with a Four-inch-thick Compact Tension Specimen*, HEDL-TME 75-10, Hanford Engineering Development Laboratory, Richland, Wash. (January 1975).
37. R. H. Bryan et al., *Tests of 6-in.-thick Pressure Vessels, Series 2: Intermediate Test Vessels V-3, V-4, and V-6*, ORNL-5059 (November 1975).
38. T. R. Mager, S. E. Yanichko, and L. R. Singer, *Fracture Toughness Characterization of HSST Intermediate Pressure Vessel Material*, WCAP-8456, Westinghouse Electric Corporation, Pittsburgh, Pa. (December 1974).
39. J. G. Merkle, G. D. Whitman, and R. H. Bryan, *An Evaluation of the HSST Program Intermediate Pressure Vessel Tests in Terms of Light-Water Reactor Pressure Vessel Safety*, ORNL/TM-5090 (November 1975).
40. J. G. Merkle et al., *Test of 6-in.-thick Pressure Vessels, Series 3: Intermediate Test Vessel V-7*, ORNL/NUREG-1 (August 1976).
41. J. A. Davidson et al., *The Irradiated Dynamic Fracture Toughness of ASTM A533, Grade B, Class 1 Steel Plate and Submerged-Arc Weldment*, WCAP-8775, Westinghouse Electric Corporation, Pittsburgh, Pa. (October 1976).
42. R. D. Cheverton, *Pressure Vessel Fracture Studies Pertaining to a PWR LOCA-ECC Thermal Shock: Experiments TSE-1 and TSE-2*, ORNL/NUREG/TM-31 (September 1976).
43. J. G. Merkle et al., *Test of 6-inch-thick Pressure Vessels, Series 4: Intermediate Test Vessels V-5 and V-9*, ORNL/NUREG-7 (August 1977).
44. J. A. Williams, *The Ductile Fracture Toughness of Heavy Section Steel Plate*, Hanford Engineering Development Laboratory, Richland, Wash. (September 1979).
45. R. H. Bryan et al., *Test of 6-in.-thick Pressure Vessels, Series 3: Intermediate Test Vessel V-7A under Sustained Loading*, ORNL/NUREG-9 (February 1978).
46. R. D. Cheverton and S. E. Bolt, *Pressure Vessel Fracture Studies Pertaining to a PWR LOCA-ECC Thermal Shock: Experiments TSE-3 and TSE-4, and Update of TSE-1 and TSE-2 Analysis*, ORNL/NUREG-22 (December 1977).
47. D. A. Canonico, *Significance of Reheat Cracks to the Integrity of Pressure Vessels for Light-Water Reactors*, ORNL/NUREG-15 (July 1977).
48. G. C. Smith and P. P. Holz, *Repair Weld Induced Residual Stresses in Thick-Walled Steel Pressure Vessels*, NUREG/CR-0093 (ORNL/NUREG/TM-153) (June 1978).
49. P. P. Holz and S. W. Wismer, *Half-Bead (Temper) Repair Welding for Heavy-Section Steel Technology Pressure Vessels*, NUREG/CR-0113 (ORNL/NUREG/TM-177) (June 1978).

50. G. C. Smith, P. P. Holz, and W. J. Stelzman, *Crack Extension and Arrest Tests of Axially Flawed Steel Model Pressure Vessels*, NUREG/CR-0126 (ORNL/NUREG/TM-196) (October 1978).
51. R. H. Bryan et al., *Test of 6-in.-Thick Pressure Vessels, Series 3: Intermediate Test Vessel V-7B*, NUREG/CR-0309 (ORNL/NUREG-38) (October 1978).
52. R. D. Cheverton, S. K. Iskander, and S. E. Bolt, *Applicability of LEFM to the Analysis of PWR Vessels Under LOCA-ECC Thermal Shock Conditions*, NUREG/CR-0107 (ORNL/NUREG-40) (October 1978).
53. R. H. Bryan et al., *Test of 6-in.-Thick Pressure Vessels, Series 3: Intermediate Test Vessel V-8*, NUREG/CR-0675 (ORNL/NUREG-58) (December 1979).
54. R. D. Cheverton, S. K. Iskander, *Application of Static and Dynamic Crack Arrest Theory to TSE-4*, NUREG/CR-0767 (ORNL/NUREG-57) (June 1979).
55. J. A. Williams, *Tensile Properties of Irradiated and Unirradiated Welds of A533 Steel Plate and A508 Forgings*, NUREG/CR-1158 (ORNL/Sub-79-50917/2), Hanford Engineering Development Laboratory, Richland, Wash. (July 1979).
56. K. W. Carlson and J. A. Williams, *The Effect of Crack Length and Side Groove on the Ductile Fracture Toughness Properties of ASTM A533 Steel*, NUREG/CR-1171 (ORNL/Sub-79/50917/3) Hanford Engineering Development Laboratory, Richland, Wash. (October 1979).
57. P. P. Holz, *Flaw Preparations for HSST Program Vessel Fracture Mechanics Testing: Mechanical-Cyclic Pumping and Electron-Beam Weld-Hydrogen-Charge Crack Schemes*, NUREG/CR-1274 (ORNL/NUREG/TM-369) (May 1980).

ACKNOWLEDGMENTS

The work described in this report was performed with funds provided by the Heavy-Section Steel Technology (HSST) program under sponsorship of the U. S. Nuclear Regulatory Commission (NRC). The author gratefully acknowledges the encouragement provided by many individuals: R. D. Cheverton, G. D. Whitman, R. H. Bryan, and J. G. Merkle. The author gratefully acknowledges the help and support that W. G. Dodge has provided in connection with the ADINA code. Acknowledgment is also due R. S. Wallace for his assistance with many of the computations and P. G. Fowler for generating the 3-D plots.

LIST OF FIGURES

LIST OF FIGURES (Contd.)

LIST OF TABLES

NOMENCLATURE

Latin Characters

a	Crack length or crack radius
A	Crack area
B	Strain-displacement transformation matrix
d_{ii}	A term on the diagonal of the stress-strain transformation matrix
D	Diagonal matrix or stress-strain transformation matrix
E	Young's modulus of elasticity
f'_i	Modified right-hand side of the upper triangularized matrix
F	Total force
F_B	Body force per unit volume
F_e	Nodal forces statically equivalent to the body forces plus the surface tractions
F_0	Nodal forces statically equivalent to the thermal plus initial strains
G	Potential energy released per unit extension or crack area (the so-called energy release "rate")
G	Modulus of rigidity
K_I, K_{I2D}, K_{I3D}	Stress intensity factor, in 2-D and 3-D, respectively
ℓ	Length parameter
L	Lower triangular matrix
N	Field to nodal values transformation matrix (interpolating functions)
P	Potential energy of the structure
Q	Thermal strain energy of the structure
r	Distance to crack root in polar coordinate system

Latin Characters (Contd.)

T	Surface traction per unit area
u	Generalized nodal displacements
u_n, u_z	Nodal displacements in the n- and z-directions, respectively
u'	Generalized displacement field
U	Upper triangular matrix
V	Volume
w	Width parameter
W	Strain energy density function

Greek Characters

α	Coefficient of linear expansion
ε	Generalized strain matrix
ε_0	Initial or thermal strain matrix
ν	Poisson's ratio
σ	Generalized stress matrix
σ_{nz}	Stresses in the n- and z-directions, respectively
τ_{nz}	Shear stress in the n-z direction
θ	Polar angle between n- and r-directions
ϕ	Angular location of a point on the crack front

Abbreviations and Acronyms	
2-D, 3-D	Two- and three-dimensional
ADINA	An FE computer code for Automatic Dynamic Incremental Nonlinear Analysis
ASTM	American Society for Testing and Materials
CPU	Central Processor Unit
DOF	Degrees of freedom
FE	Finite element(s)
FMECH	A 2-D FE based computer code to calculate K_I using energy release methods
GEN8	An FE mesh generation computer code
HEATING5	A finite difference based heat conduction computer code
HSST	Heavy-Section Steel Technology
IO	Input or output computer operation
LEFM	Linear elastic fracture mechanics
MERGE	An FE mesh generation computer code
NRC	Nuclear Regulatory Commission
ORNL	Oak Ridge National Laboratory, Oak Ridge, Tennessee
PE	Potential energy
QMESH	An FE mesh generation
REDUCE	An FE mesh node-numbering optimizer
STRIP	An FE mesh generation computer code
TSE-4	The fourth thermal shock experiment
V8	An FE mesh generation computer code
V-8	One of the experimental test cylinders of the HSST program

TWO FINITE ELEMENT TECHNIQUES FOR COMPUTING MODE I STRESS INTENSITY FACTORS IN TWO- OR THREE-DIMENSIONAL PROBLEMS

S. K. Iskander

ABSTRACT

Two finite element (FE) approaches were used to calculate opening mode I stress intensity factors (K_I) in two- and three-dimensional (2-D and 3-D) problems for the Heavy-Section Steel Technology (HSST) program. For problems that can be modeled in two dimensions, two techniques were used. One of these may be termed an "energy release rate" technique, and the other is based on the classical near-tip displacement and stress field equations. For three-dimensional problems, only the latter technique was used.

In the energy release technique, K_I is calculated as the change in potential energy of the structure due to a small change in crack length. The potential energy is calculated by the FE method but without completely solving the system of linear equations for the displacements. Furthermore, the system of linear equations is only slightly perturbed by the change in crack length and, therefore, many computations need not be repeated for the second structure with the slight change in crack length. Implementation of these last two items has resulted in considerable savings in the calculation of K_I as compared to two complete FE analyses. These ideas are incorporated in the FMECH code.

The accuracy of the methods has been checked by comparing the results of the two approaches with each other and with closed form solutions. It is estimated that the accuracy of the results is about ±5%.

1. INTRODUCTION

Flaws in structural components may occur during the fabrication processes or after the component has been put into service. Such flaws may escape detection in inspection. An important consideration in the design and analysis of such structural components is the stability of such flaws not only under normal operating conditions, but under hypothetical accident conditions.

Among the significant parameters in judging the propensity of flaws to propagate is the stress intensity factor, which depends upon the geometry and loading of the structure. These factors may be classified into three basic types, each associated with a local mode of deformation near the crack tip as shown in Figure 1 [1]. Conceptually, the methods described in this report can be used for the determination of the stress intensity factor associated with any of the three modes. This report, however, deals with the opening mode I type of deformation, which implies a loading symmetric with respect to the plane of the crack. All the methods described are based upon the basic assumptions of linear-elastic fracture mechanics (LEFM), viz., that all nonlinear effects are confined to a "small" region surrounding the crack tip and, consequently, may be neglected. A linear elastic analysis then approximates the essential features of such cases.

The number of "closed" form solutions in LEFM are limited. For the case of an arbitrarily shaped structure subjected to a general system of loads, numerical methods are used. There are many such methods, among which the influence function [2], the boundary integral [3], and the FE [4] approaches are noteworthy. Of these approaches, the ones based

DWG. NO. K/G-80-2164
(U)

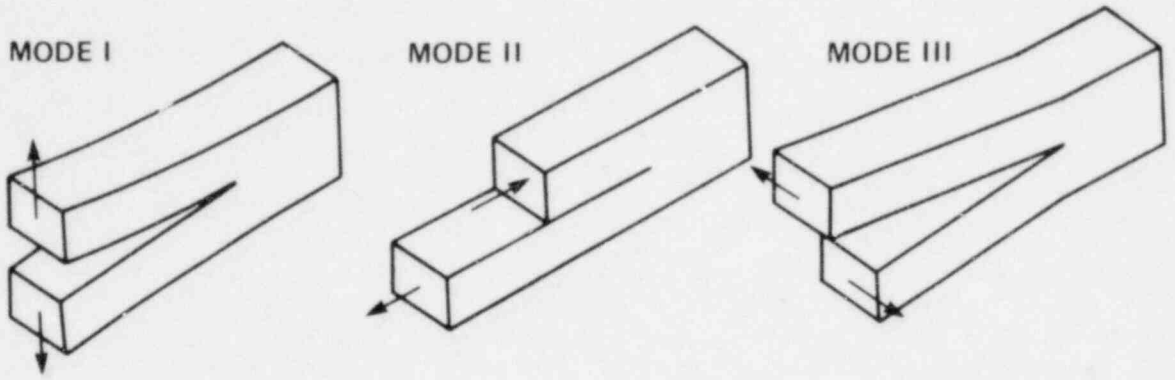

Figure 1. The three basic modes of deformation associated with cracks

upon FE have been particularly popular due to the widespread availability of general-purpose computer codes, and this report discusses the implementation of two FE procedures used to calculate K_I. One of these is based upon the so-called energy release concept of LEFM and the other on the classical relationship between the near-tip stress (or displacement) fields and the stress intensity factor K_I.[1] The energy release rate concept has been used with our 2-D models only, whereas the stress/displacement method has been used with both our 2-D and 3-D models. Verification of the methods has been carried out by comparison with closed form solutions and by comparing the results of the two different FE approaches for the 2-D problems.

The objective of this report is to document the energy release and stress/displacement methods as they have been implemented for the HSST program. Thus, in Chapter 2 two approaches based upon the energy release method are presented. The first approach is labeled the potential energy method, whereas the second one is termed the strain energy method. It is shown that, for special cases of either external loads only or thermal gradients only, both methods give the correct stress intensity factor. In cases where both types of loads are present, the strain energy approach will lead to erroneous results. Also presented is the complete derivation of a simple procedure to extract the potential energy from the upper triangularized system of equations arising in FE methods without solving explicitly for the displacements. The stress/displacement method is also documented.

---

[1] This method will be referred to as the stress/displacement method for brevity.

In Chapter 3, results from several 2- and 3-D examples are presented. First, as partial verification of the methods given in Chapter 2, a problem for which a closed form solution exists was solved in both 2-D and 3-D cases. Second, in 2-D cases, both the potential energy and stress/displacement methods were used to solve the same problem. In all cases, the results were within a few percentage points of the closed form solution or each other. Also presented are the results of two 3-D analyses performed for the HSST program. The first analysis explores, for several different cylinder lengths, the variation of K_I along the length of a uniform depth axial crack in a cylinder subjected to a thermal shock. The second deals with the variation of K_I along the crack front for several different load cases of the V-8 cylinder.

One important task in the FE modeling--that of mesh generation--is also one of the most time-consuming. Many codes have been developed by the author to facilitate this task and they will be mentioned briefly. The method used in optimizing the profile of the system of linear equations occurring in our 3-D FE analysis is also mentioned. Optimization is critical since, in many cases, analysis would not be possible due to limitations imposed by the computer environment.

2. METHODS OF ANALYSIS

2.1. Introduction

In this chapter, both the energy release rate and the stress/displacement methods will be discussed.

2.2. Energy Release Rate Methods

This section presents the basis of the energy release rate method for calculation K_I as it is implemented in the FMECH code. This method relies upon the calculation of the PE of the structure, and this is accomplished by means of the FE method. A brief derivation of the governing equations of the FE method based upon PE considerations is first given. These equations will be referred to in a discussion of the errors that arise if the strain energy is used in place of the potential energy in situations where both thermal and mechanical loads act on the structure (since some authors have used the strain energy release rate to calculate K_I). The governing equations of the FE method are also referred to in reviewing an economical computational method for calculating the PE. It is shown that the PE of the structure is available at the end of the forward elimination process and, hence, if the displacements or stresses are not required, the FE solution can be terminated at this point, thereby saving the cost of back substitution and the cost of computing the displacements and stresses.

One of the earliest papers in fracture mechanics was that of Griffith [5]. It introduced the concept of energy release due to the propagation of cracks in brittle materials. Later, Irwin [6] and

Orowan [7] extended Griffith's work to account for the "small" plastic zone ahead of the crack tip; so this concept may also be termed the Griffith-Irwin-Orowan theory.

Let P be the total potential energy (PE) of deformation of a structure, and $G\ dA$ be the total elastic energy made available when the crack extends by an amount dA, where A is the crack surface area (one side of the crack); then

$$G = -\frac{dP}{dA} \tag{1}$$

Furthermore, Irwin [8] showed that

$$G = \frac{1}{E} K_I^2 \qquad \text{for plane stress}$$

$$\text{and } G = \frac{1 - \nu^2}{E} K_I^2 \qquad \text{for plane strain} \tag{2}$$

where

K_I = opening mode stress intensity factor,

E = modulus of elasticity,

ν = Poisson's ratio.

Thus, it is possible to estimate K_I by evaluating the change in the PE of a structure (ΔP) due to a small extension of the crack surface (ΔA).

There are various approaches to implementing energy methods using FE analysis. One approach would be to perform an FE analysis on the cracked structure, then extend the crack by a small amount and perform a second FE analysis, thus determining the PE corresponding to each crack length [9]. The disadvantage of this method is the necessity of having to perform two complete FE analyses.

Rather than perform two complete and separate FE analyses to obtain K_I, it is possible to optimize the process in a manner that reduces the costs to an amount equal to or less than that for a single complete FE analysis. In describing this optimization, many of the basic equations of the FE method will be referred to and, therefore, they will now be reviewed from a PE viewpoint although such a derivation is common in the FE literature.

The total PE of a structure is given by [11, p. 384]

$$P = \int_{vol} W \, dV - \int_{vol} u' \, F_B \, dV - \int_{area} u' \, T \, dA \quad , \tag{3}$$

where

W = strain energy density,

u' = displacement field,

F_B = body forces per unit volume,

T = surface tractions per unit area.

The first term is the internal strain energy and the remaining two terms are the work done by the external forces.

Equation (3) will be rewritten in a form suitable for FE analysis.

The strain energy density can be expressed as[2]

$$W = \frac{1}{2}(\varepsilon - \varepsilon_0)^T D(\varepsilon - \varepsilon_0) \quad ,$$

[2]Vectors and matrices will not be given any special symbol (e.g., $\{\varepsilon_0\}$ or $[D]$) since their definition and context of their use make their meaning unambiguous.

where

ε = total strain vector,

ε_0 = thermal and/or initial strain vector, and superscript T denotes transpose,

D = matrix of the stress-strain transformation matrix, i.e., $\sigma = D(\varepsilon - \varepsilon_0)$, σ = stress vector.

Let $\varepsilon = B\,u$, where

u = nodal displacement vector,

B = strain-displacement transformation matrix.

Then for the structure

$$\int W\,dV = \frac{1}{2}\,u^T \int_{vol} B^T D\,B\,dV\,u - u^T \int_{vol} B\,D\,\varepsilon_0\,dV$$

$$+ \frac{1}{2} \int_{vol} \varepsilon_0^T D\,\varepsilon_0\,dV$$

$$= \frac{1}{2}\,u^T K\,u - u^T F_0 + Q \quad ,$$

where

K = stiffness matrix for the structure

$$= \int_{vol} B^T D\,B\,dV$$

F_0 = nodal loads statically equivalent to the thermal or initial strains

$$= \int_{vol} B^T D\,\varepsilon_0\,dV$$

Q = thermal energy $= \frac{1}{2} \int \varepsilon_0^T D\,\varepsilon_0\,dV$.

Thus, the PE can be written as

$$P = \frac{1}{2}\,u^T K\,u - u^T F_0 - u^T F_e + Q \quad ,$$

where F_e are the nodal forces statically equivalent to the body forces and the surface tractions, i.e.,

$$F_e = \int_{area} N^T T \, dA + \int_{vol} N^T F_B \, dV$$

where N = the interpolating functions relating the displacement field within an element to its nodal displacements, viz., $u' = N u$.

Thus, the PE can be written in the form

$$P = \frac{1}{2} u^T K u - u^T F + Q \tag{4}$$

where $F = F_e + F_0$ (the sum of the external loads F_e and the initial or thermal loads F_0).

The use of the theorem of minimum potential energy, viz., the first variation on P with respect to the displacement δu [11, p. 382]

$$\text{viz., } \delta P = 0 \quad \text{leads to}$$

$$K u = F \tag{5}$$

Equation (5) forms the basis for the FE method. Substituting for F from Eq. (5) into Eq. (4)

$$P = \frac{1}{2} u^T K u - u^T K u + Q$$

or

$$P = -\frac{1}{2} u^T K u + Q \tag{6}$$

Recall that the term Q depends upon the thermal strains ε_0 and the material properties D. The ε_0 are functions of temperature and the coefficient of thermal expansion (which is not contained in D) only. The term Q is therefore independent of the boundary conditions. Thus, the

change in PE with respect to a change in crack area can be written as

$$G = -\frac{dP}{dA} = \frac{d}{dA}\left(\frac{1}{2} u^T K u\right) \tag{7}$$

In the absence of external mechanical loads, the PE of a structure, Eq. (3), is given by $\int W\, dV$, the internal strain energy of the structure. On the other hand, if there are no thermal stresses, the strain is equal to the work done by the external forces[3] (Clapeyron's Theorem [11, p. 86]). In both these cases, the use of the strain energy in place of the PE in Eq. (1) is valid, except for the sign. This has lead many authors [1,12] to use the term "strain energy release rate" in place of the "potential energy release rate." Where both external and thermal loads act on a structure, the use of strain energy can lead to errors, since this does not account for the work done by thermal expansion on the external loads.

For example, consider a bar supported at one end in such a manner that a uniform temperature change only causes a stress-free thermal expansion. If the bar is subjected to external mechanical loads, a uniform temperature change will cause no change in the strain energy, but will alter the PE of the structure.

As mentioned above, one obvious and straightforward method of calculating K_I by the energy release rate method would be to perform two complete and separate FE analyses. However, two simplifications are possible. First, the element stiffnesses calculated for the first FE analysis are saved and, since they are a function of the dimensions and material properties only, they may be utilized in the second FE analysis

---

[3] Mathematically expressed as $\int_{vol} u' F_B\, dV + \int_{area} u' T\, dA = 2 \int W\, dV$.

and only the boundary conditions are modified to account for the new crack root. Since the cost of the calculation of the element stiffness comprises a major portion of the cost of an FE analysis, the savings are significant.

The second simplification concerns the solution of Eq. (5) and the computation of the displacements and stresses. About half the cost associated with these operations can be saved by means of a scheme due to Hellen [10]. It is shown that the PE of the structure is available at the end of the forward elimination process and thus, if the displacements or the stresses are not required, their costs can be eliminated by terminating the FE computation at this point. Basically, this scheme enables the computation of the term (u^T K u) or, equivalently, the work done by the total forces acting through their corresponding displacements (F^T u). The method relies upon the symmetry of the stiffness matrix K and upon the ability to decompose the matrix into the following form [13]

$$K = L\ D\ U \quad , \tag{8}$$

where L and U are lower and upper triangular matrices with units along their principal diagonals, and D is a diagonal matrix whose elements are the "pivots" of Gaussian elimination. Moreover, since K is symmetric, $U = L^T$. Then

$$K = L\ D\ L^T \tag{9}$$

The solution of Eq. (5) then proceeds as follows:

$$K\ u = F$$

or

$$L\ D\ L^T\ u = F$$

Forward elimination is symbolically represented as:

$$D\,L^T\,u = L^{-1}\,F \tag{10a}$$

or, if the pivots are reduced to unity, then

$$L^T\,u = D^{-1}\,L^{-1}\,F \tag{10b}$$

For brevity, let

$$F'' = L^{-1}\,F$$

and

$$F' = D^{-1}\,L^{-1}\,F$$

then

$$L^T\,u = F'$$

In other words, F' (or F") is the state of the total force vector at the end of the forward elimination process. The remaining back substitution process is symbolized as

$$u = L^{T^{-1}}\,F' \tag{11}$$

then

$$u^T\,K\,u = (F'^T\,L^{-1})\,(L\,D\,L^T)\,(L^{T^{-1}}\,F')$$

$$= F'^T\,D\,F' \tag{12a}$$

or

$$u^T\,K\,u = F''^T\,D^{-1}\,F'' \tag{12b}$$

Here the form (12b) would be used if, at the end of the forward elimination, the pivots had been normalized; otherwise, (12a) would be used.

Thus,

$$u^T K u = \sum_{i=1}^{n} (f_i')^2 d_{ii} \qquad (13)$$

In other words, the above sum can be accumulated during the forward elimination process and there is no need to carry out the back substitution stage or its attendant cost in CPU[4] and IO,[5] nor is there a need to calculate either the displacements or the stresses.

There are many advantages to the energy method and these have been documented in detail in [9]. For a given mesh, energy methods give better accuracy than stress/displacement methods and they are insensitive to a large extent to the details of the mesh layout. This may be due to errors that cancel out since the meshes used in both analyses (the first with a crack length A and the second with a crack length of $(A + \Delta A)$ are identical except for the boundary conditions on the crack front. A significant advantage is also the high degree of automation which energy methods lend themselves to, as contrasted with the stress or displacement methods mentioned later.

---

[4]CPU = Central Processor Unit--used synonomously for computations.

[5]IO = Input or Output operations to disks or tapes.

2.3. Stress and Displacement Methods

These methods rely upon the classical relationships between the near field solution and the stress intensity factor K_I [14] (see Figure 2 for coordinate system notation). The stresses are given by

$$\sigma_n = \frac{K_I}{(2\pi r)^{1/2}} \cos\frac{\theta}{2}\left[1 - \sin\frac{\theta}{2}\sin\frac{3\theta}{2}\right] + \ldots$$

$$\sigma_z = \frac{K_I}{(2\pi r)^{1/2}} \cos\frac{\theta}{2}\left[1 + \sin\frac{\theta}{2}\sin\frac{3\theta}{2}\right] + \ldots$$

$$\tau_{nz} = \frac{K_I}{(2\pi r)^{1/2}} \sin\frac{\theta}{2}\cos\frac{\theta}{2}\cos\frac{3\theta}{2} + \ldots \qquad (14a)$$

The displacements are (assuming plane strain conditions)

$$u_n = \frac{K_I}{G}\left(\frac{r}{2\pi}\right)^{1/2} \cos\frac{\theta}{2}\left(1 - 2\nu + \sin^2\frac{\theta}{2}\right) + \ldots$$

$$u_z = \frac{K_I}{G}\left(\frac{r}{2\pi}\right)^{1/2} \sin\frac{\theta}{2}\left(2 - 2\nu - \cos^2\frac{\theta}{2}\right) + \ldots \qquad (14b)$$

where ... represent terms of order r and $r^{(2n+1)/2}$ $(n = 0,1,\ldots,\alpha)$ that are small with respect to the first term when r becomes small,

G = modulus of rigidity = $E/2(1 + \nu)$ for isotropic materials,

ν = Poisson's ratio,

E = Young's modulus of elasticity.

In the region close enough to the crack, K_I is calculated from Eq. (14a) or (14b). If the displacements are used, by taking $\theta = \pi$, we get

$$K_I = \frac{E\sqrt{2\pi}}{4(1 - \nu^2)}\left(\frac{u_z}{\sqrt{r}}\right) \qquad (15)$$

ORNL Dwg. 79-5916 ETD

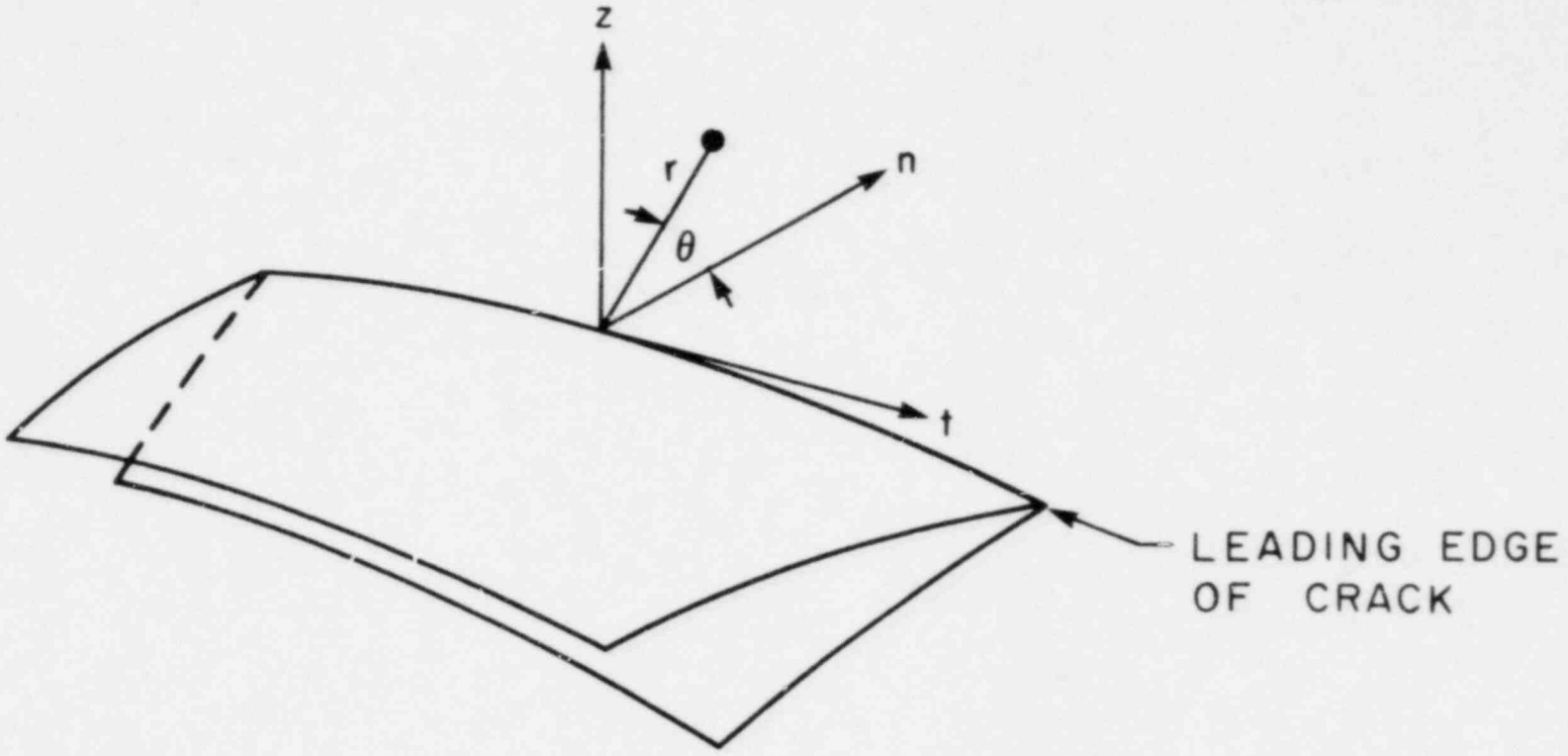

Figure 2. The two coordinate systems of axes used. The orientation of the axes is determined by the tangent (t) to the crack root edge and the normal (n) to the crack edge, with both (t) and (n) in the plane of the crack. The z-axis is then normal to both t- and n-axes. The polar system (r-θ) is in the n-z plane.

Similarly, if the stresses are used, by taking $\theta = 0$, we get

$$K_I = (2\pi)^{1/2} (\sigma_z \sqrt{r}) \tag{16}$$

The displacements are the primary solution in most FE computer codes. The stresses are obtained by numerical differentiation with some loss in accuracy. In the interests of accuracy, the stresses are computed at the so-called gaussian integration points, which are interior to the element and not exactly at $\theta = 0$. Thus, it may be preferable to use the displacements whenever possible. However, the stresses would be used to calculate K_I where the displacements are not available, for example, in 3-D problems in which the crack front does not intersect the free surface at a right angle.

The procedure used to calculate K_I is to plot either the term $ur^{-1/2}$ or $\sigma r^{1/2}$ as a function of r. The stresses or displacements are taken from the FE solution along a ray normal to the crack front. By extrapolating the curve back to $r = 0$, an estimate of K_I may be obtained. It has been found by solving problems with closed form solutions that a straight line extrapolation gives reasonably good results [31]. (Also see Sections 3.2.1. and 3.3.1. of this report.)

The total number of degrees of freedom (DOF) and, hence, the computational effort can be decreased considerably by the use of so-called "singularity elements" around the crack tip. These elements reproduce the $\frac{1}{\sqrt{r}}$ singularity in the stresses, thereby allowing the use of relatively few elements in the crack tip region; otherwise, the high stress gradients in that region necessitate a highly refined mesh so that these gradients can be modeled with reasonable accuracy by either constant or linear

stress elements. One type of singularity element can be produced from any element with mid-side nodes by locating the mid-side nodes adjacent to the crack front at the $\frac{1}{4}$ point (Figure 3).[6] The stresses in the element will possess the correct singularity in the stresses as well as the correct stiffness, but the displacements at the $\frac{1}{4}$ nodes will be inaccurate [16]. Such an element is often referred to as the $\frac{1}{4}$ point element.

One advantage of the energy methods mentioned is the immediate computation of K_I as compared to stress or displacement methods which require a certain amount of manual plotting and computation, thereby lending themselves to a high degree of automation.

The energy methods described above have been implemented in the finite element code FMECH (Fracture Mechanics). This code is designed to compute K_I for problems with any form of loading, mechanical or thermal. However, it is particularly useful and relatively efficient in LEFM problems with transient thermal loadings. In such cases, the aim is to calculate K_I for a large number of different temperature distributions as well as different values of the crack depth.

---

[6] Such elements were introduced almost simultaneously by Barsoum [15] and Henshell [16].

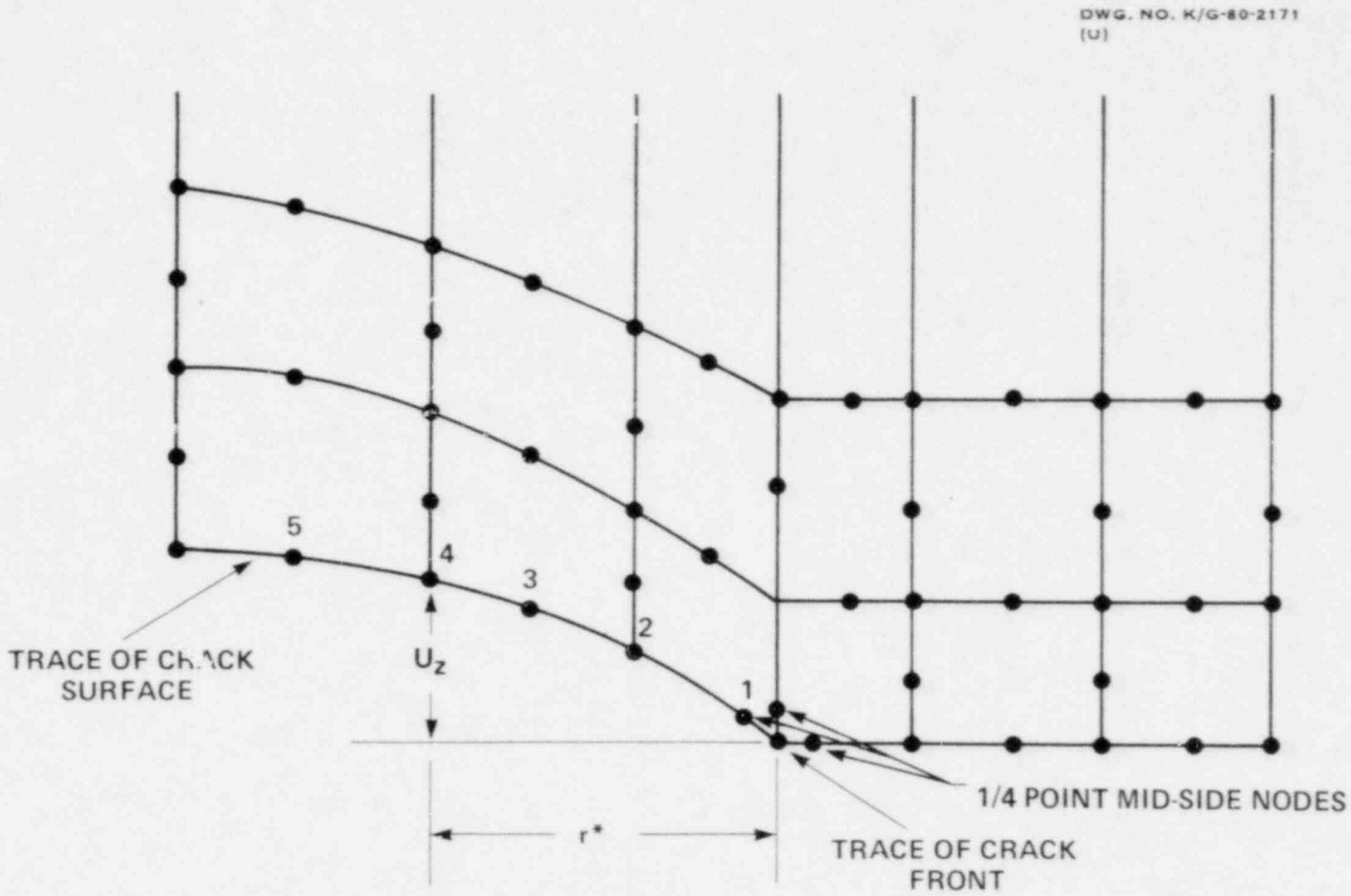

Figure 3. Quarter point singularity element. Number adjacent to the nodes refer to the FE displacements at these nodes in Table 7

3. EXAMPLES OF ANALYSIS

3.1. Introduction

This chapter presents some problems that have been solved using the techniques previously described in this report. The object of this is twofold. First, by solving problems that have either well-established or "closed form" solutions, a partial validation of the method and some assessment of the accuracy of the solution can be made. Second, it presents examples of the type of problems arising in the HSST program that have been solved with these techniques.

The first section deals with 2-D problems, the second one with 3-D problems. Both sections start with a problem for which a closed form solution exists then deal with the problems arising in the HSST program.

3.2. Two-Dimensional Examples

Two problems will be discussed in this section. The first has a closed form solution and thus gives a rough assessment of the accuracy of the stress/displacement method. The second problem, one that arises in the HSST program, was solved using all the different approaches described in this report and the results have been compared.

3.2.1. Finite Length Strip With a Central Crack

The closed form solution of the centrally cracked strip has been given by Isida [17] and has been used extensively to verify numerical solutions. Such a strip with a crack-to-width ratio (a/w) of 0.10 and a length-to-width (ℓ/w) of 3 has been modeled with 14 elements and is shown in Figure 4. The

DWG. NO. K/G-80-2316
(U)

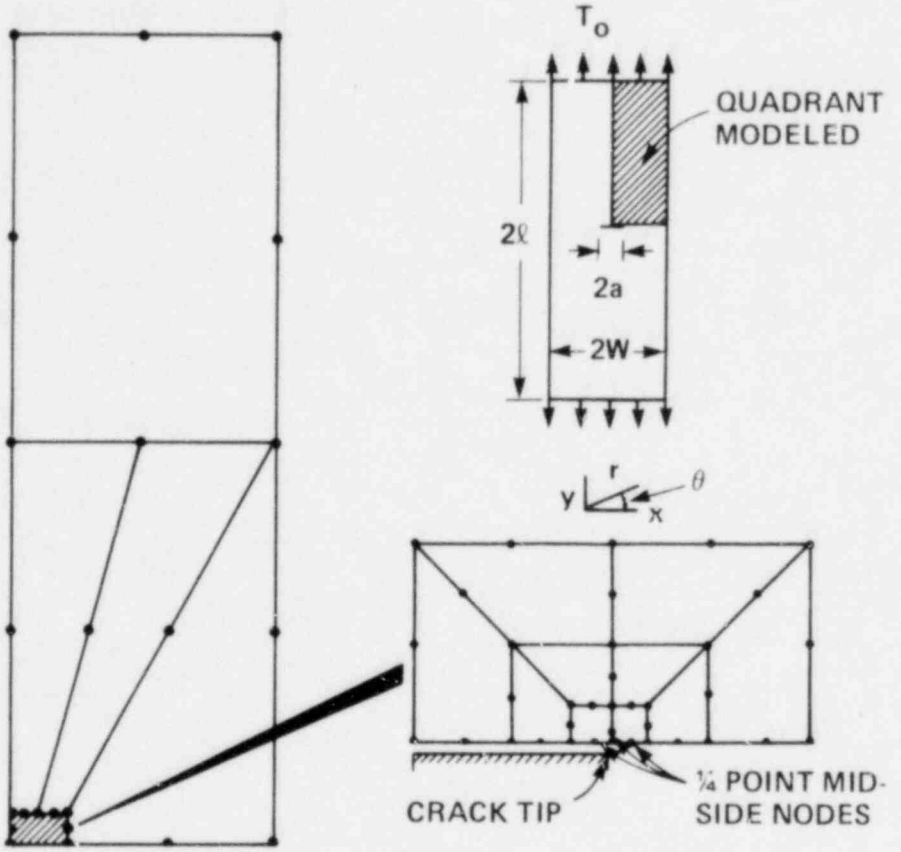

Figure 4. Finite element idealization for a centrally cracked strip

displacement method was used. The stress intensity factor K_I was normalized by dividing it by $T\sqrt{\pi a}$,[7] where T is the externally applied traction and 2a is the crack length (Figure 4). The theoretical value given by Isida is 1.006. The normalized stress intensity factor calculated from the displacements[8] is plotted against r, the distance from the crack tip, and is shown in Figure 5. The two straight-line fits give the values obtained when using either two or three integration points[9] in the FE code. The results for the two integration points are better (2% higher than theoretical) than three integration points (7% lower). Hellen [29,30] has reported results showing similar trends. Two integration points were used in all subsequent work of this type.

3.2.2. Long Axial Flaw in a Cylinder Under Thermal Shock

The cylinder analyzed is the one used in the TSE-4 experiment [19]. In this experiment, the test specimen was a cylinder of 0.533 m (21 in.) outside diameter, 0.241 m (9.5 in.) inside diameter, and 0.914 m (36 in.) long. The material was A508, class 2 with a quench only heat treatment (from 871°C). The long axial flaw was 11 mm (0.42 in.) deep. Initially, the whole cylinder was heated to 291°C (555°F) then the inside surface was suddenly cooled by a methyl alcohol/water mixture.

---

[7]The stress intensity factor for an infinite plate.

[8]All the FE analyses with the stress and displacement method were performed using the ADINA Code [18].

[9]Implying a 2 x 2 or 3 x 3 integration order in 2-D and 2 x 2 x 2 or 3 x 3 x 3 in 3-D integration order in 3-D.

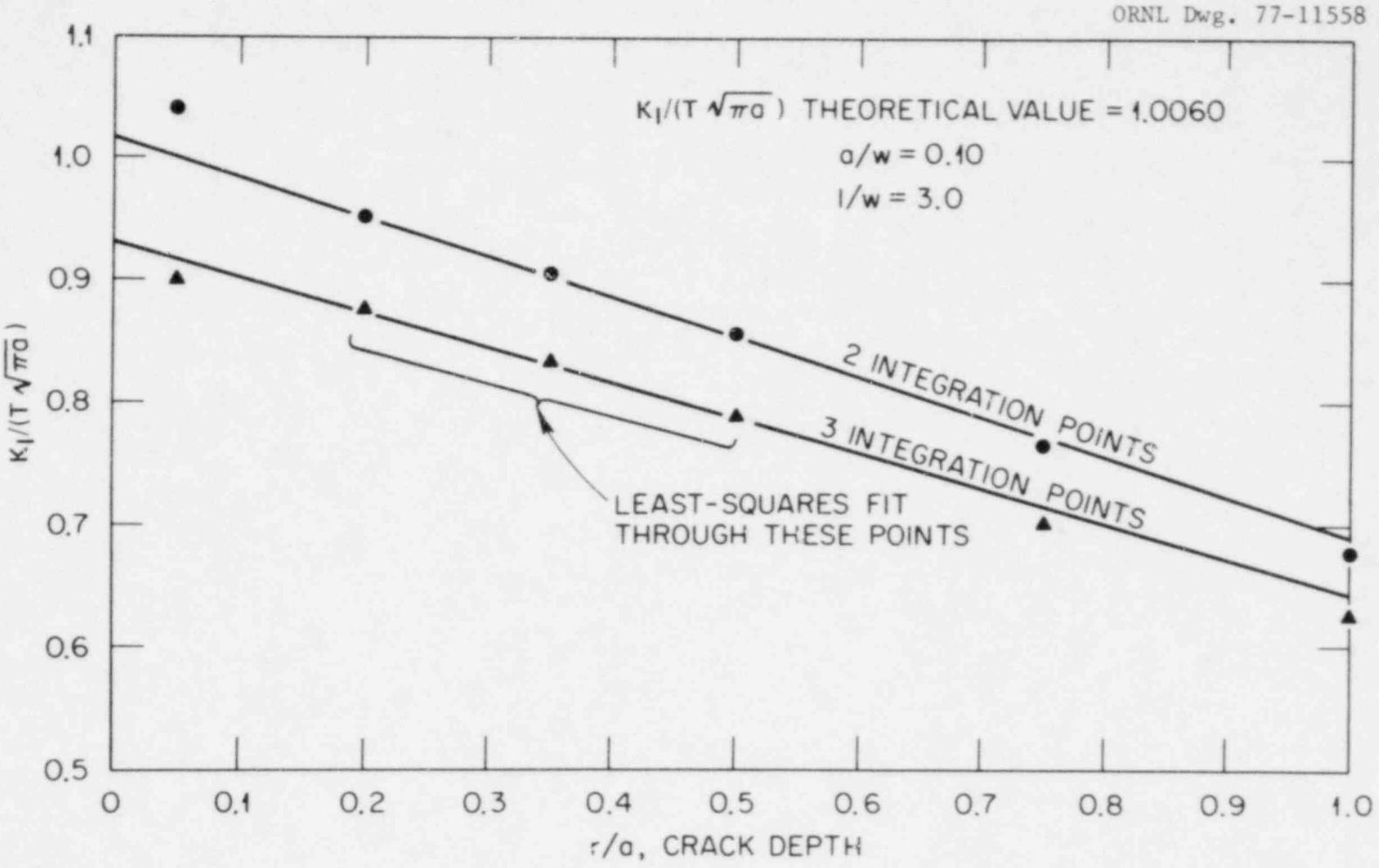

Figure 5. Estimates of K_I as calculated from nodal displacements

The coolant temperature was initially -25°C (-13°F). The actual experimental temperatures obtained by the thermocouples on the cylinder during the transient were used in the calculation of K_I. The analysis was performed using two different codes, each with different techniques. The FMECH code utilizes energy-based techniques, but two slightly differing approaches were used.

The first approach with this code, which is documented in Reference [9], may be termed the "strain" energy approach and is based upon the fact that, in the absence of external forces, the PE and the internal strain energy are identical (see Eq. (3)). The displacements and stresses are first computed by the FMECH code and then the internal strain energy term is calculated from a quadratic expression in the stresses [9]. The other approach uses a more economical method described in Section 2.2. of this report and has been termed the "potential energy" approach. A typical mesh for both approaches is shown in Figure 6.

The mesh for the displacement method using the ADINA code is shown in Figure 7. The results of the analysis using all of these different approaches are given in Table 1. The maximum difference between the K_I values for any particular time interval is 7%. The results calculated by the potential energy approach are more accurate than those obtained by the strain energy method since fewer computations are performed and, therefore, round-off errors are less.

Considering the accuracy demonstrated by the stress/displacement method in Section 3.2., the close agreement between the

DWG. NO. K/G-80-2160
(U)

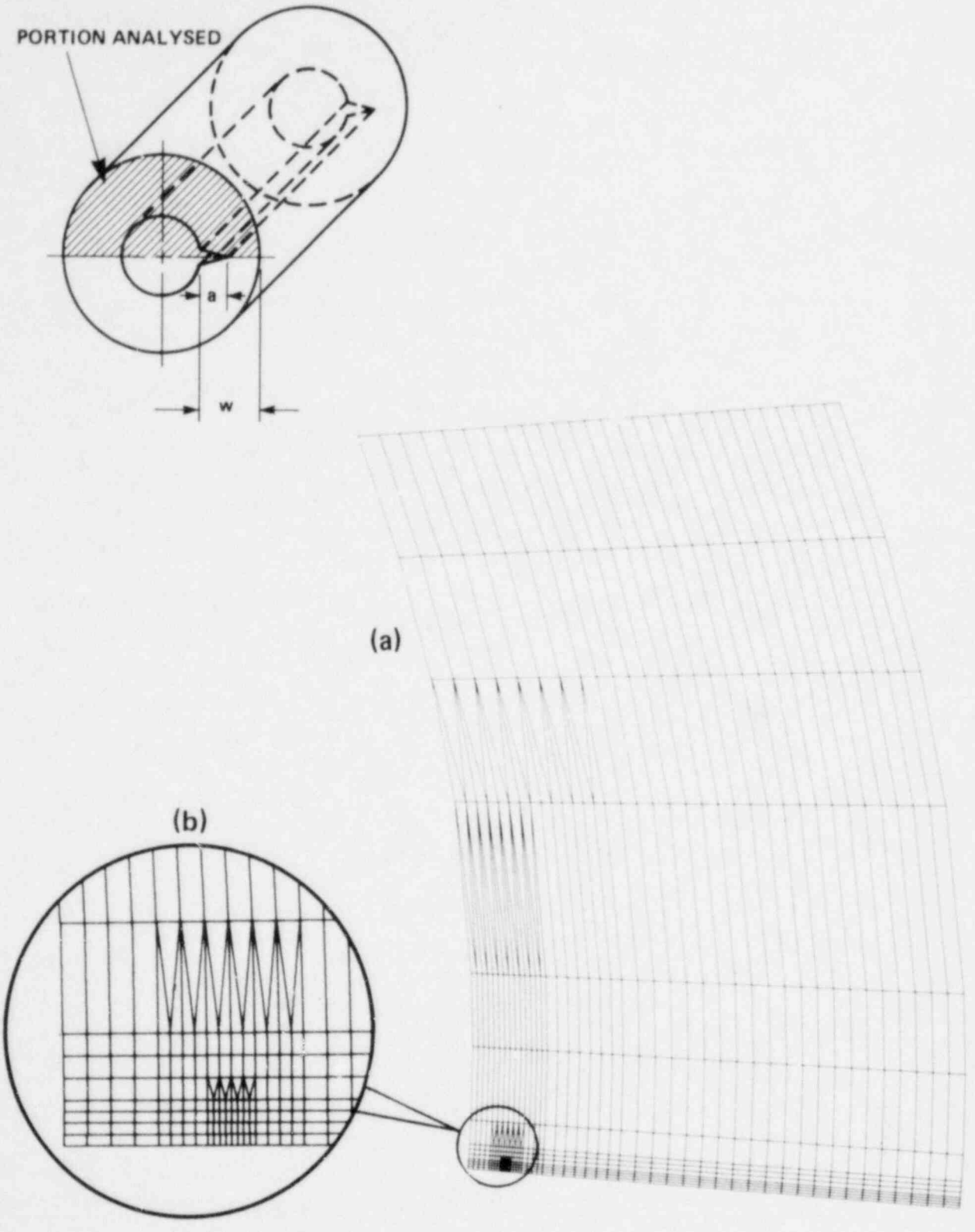

Figure 6. A typical FE mesh used with energy release methods

DWG. NO. K/G-80-2159
(U)

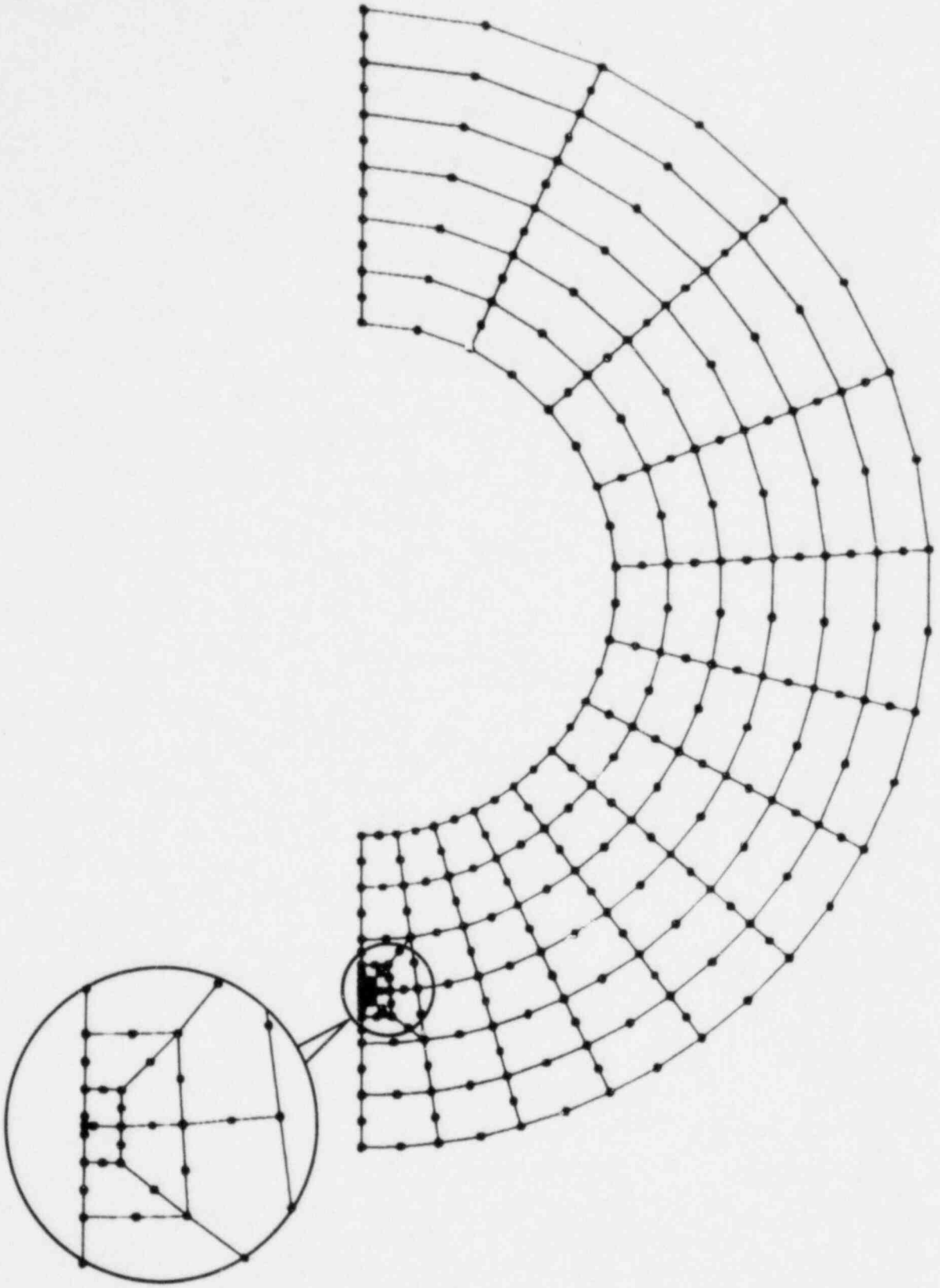

Figure 7. A typical model for use with displacement or stress methods

Table 1

Comparison of K_I obtained by energy release rate methods to those obtained by the displacement method

	K_I MPa·m$^{1/2}$ (ksi·m$^{1/2}$)		
Time in Transient (Minutes)	0.4	5.03	15.03
Energy Release Rate Methods (FMECH Code)			
Strain Energy	26.9 (24.5)	94.3 (85.8)	69.0 (62.8)
Potential Energy	27.8 (25.3)	97.1 (88.4)	71.1 (64.7)
Displacement Method (ADINA Code)			
251 Nodes	25.1 (22.8)	90.7 (82.5)	66.5 (60.5)
625 Nodes	25.5 (23.2)	91.2 (83.0)	66.9 (60.9)

stress/displacement and the energy methods also indicates that the energy method gives good accuracy.

The main advantage of the energy method over the stress/displacement method is the high degree of automation that the former one lends itself to. Stress/displacement methods as described in this report require some manual effort: extracting the stresses or displacements at the proper locations, calculating the K_I values, plotting and extrapolating the values to r = 0. Some of this effort may be eliminated by automating some of it. However, an element of judgment will always still be required in fitting the straight line through the data points. The energy method on the other hand yields K_I values immediately.

3.3. Three-Dimensional Examples

In this section, analyses of some 3-D problems will be presented. Although the stress/displacement method is easily applied to 3-D problems, the usual difficulties of generating 3-D FE meshes become more acute in 3-D crack problems in which it is difficult to obtain the number of nodes necessary for a reasonable degree of accuracy and still remain within the available computer capacity. Some of the problems described here were close to the maximum size problems that could be handled with the software and hardware existing at the time.

A brief description of the mesh generation process is given in Appendix A, and the details of the FE modeling and analysis are given in Appendix B.

The questions of validating the model and the mesh for 3-D problems are the same as for 2-D problems. Partial verification of the overall method was obtained by solving the 3-D problem of an imbedded plane circular crack located centrally in a cylinder which has a closed form solution. The other examples presented are problems arising in the HSST program.

One of these problems, that of the variation of K_I axially along a longitudinal crack of uniform depth in cylinders of differing lengths, implicitly provides some verification of the results since, as the length increases, the stress intensity factors at mid-length should approach those of the corresponding 2-D plane strain problem.

Another problem presented arose during the pretest analysis of the V-8 cylinder. A part-through crack was to be produced on the outside surface of a cylinder in an HSST program test whose purpose was the determination of the influence of a residual stress field on the behavior of a flaw in a pressurized vessel.

3.3.1. Plane Circular Crack Located Centrally in a Cylinder

The closed form solution for the case of a long cylinder subjected to a uniform axial tensile load applied at the ends and stress-free cylindrical sides and a centrally located plane circular crack was obtained by Sneddon and Welch [20]. Values of K_I from that solution for Poisson's ratio of 0.25 have been reproduced in a graphical form by Rooke [21]. A particular case of such a cylinder was modeled and analyzed. Table 2 gives the dimensions, material properties, and loading used in the analysis. The axisymmetry of the problem allows a sector of any angular

Table 2

Dimensions and material properties used in the analysis of centrally cracked cylinder

Dimensions	
Radius of cylinder	254 mm (10 in.)
Cracked radius	127 mm (5 in.)
Distance from crack plane to ends	812.8 mm (32 in.)
Material Properties	
Young's modulus E	200 GPa (29 x 10^6 psi)
Poisson's ratio ν	0.25
Loading	
End traction	68.9 MPa (10 ksi)

dimension to be analyzed, but the restrictions imposed by the code[10] lead to the choice of a quarter of the cylinder to be modeled. Figure 8 shows the 2-D mesh used to generate the 3-D model shown in Figure 9. Details of the FE modeling and analysis are given in Appendix B.

The nodal displacements from the FE analysis are given in Table 3. As an illustration of the process of estimating K_I from these displacements, the term $u_z r^{-1/2}$ has been plotted in Figure 10. A best fit straight line extrapolated to r = 0 gives a value of

$$u_z r^{-1/2}\Big|_{r=0,\ \theta=\pi} = 7.14 \times 10^{-3}\ \text{mm}^{1/2}\ \ 1.42 \times 10^{-3}\ \text{in}^{1/2} \quad ,$$

and the use of expression (15) yields a value of

$$K_I = 30.2\ \text{MPa} \cdot \text{m}^{1/2} (27.5\ \text{ksi} \cdot \text{in}^{1/2})$$

When this value is normalized by dividing by $2T\sqrt{a/\pi}$, the stress intensity factor for a plane circular crack of radius a in an infinite medium subjected to a uniform stress of T gives a value of 1.088. Rooke [19] gives a corresponding value of 1.074. Thus, the method gives values within 1.5% of the closed form solution. No convergence studies with differing mesh sizes were performed to insure that this result is not fortuitous. However, in the V-8 analysis described later in this report, convergence studies with a mesh similar to this one and a mesh with 50% more nodes

[10] In the ADINA code, boundary conditions at the planes of symmetry can only be applied in directions parallel to the x-y-z coordinate axes.

DWG. NO. K/G-80-2166
(U)

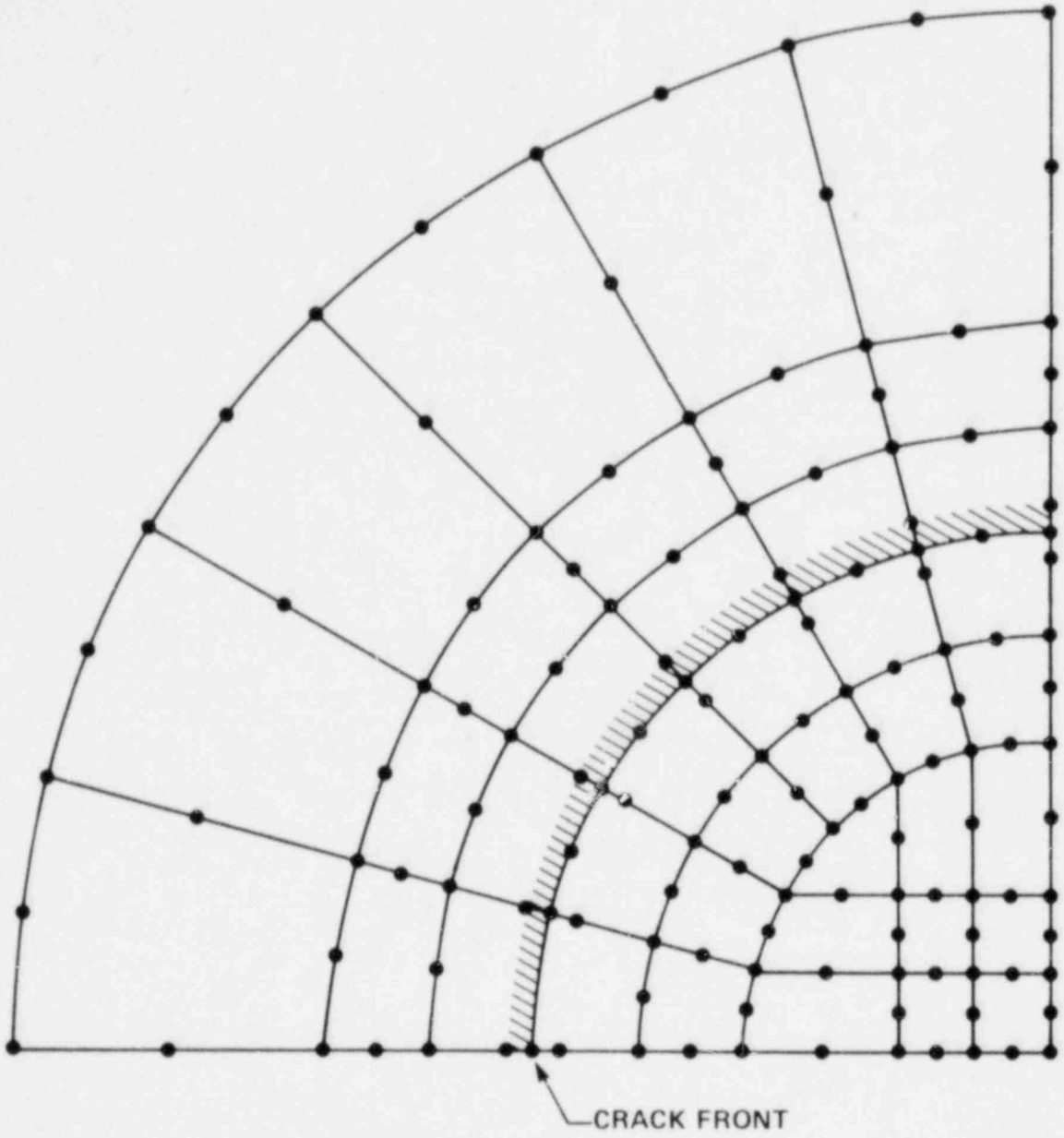

Figure 8. Two-dimensional mesh used to generate the 3-D FE mesh by propagating it normal to the plane of the paper. The resulting 3-D mesh, shown in Figure 9, was used for the analysis of the circular central crack

DWG. NO. K/G-80-2176
(U)

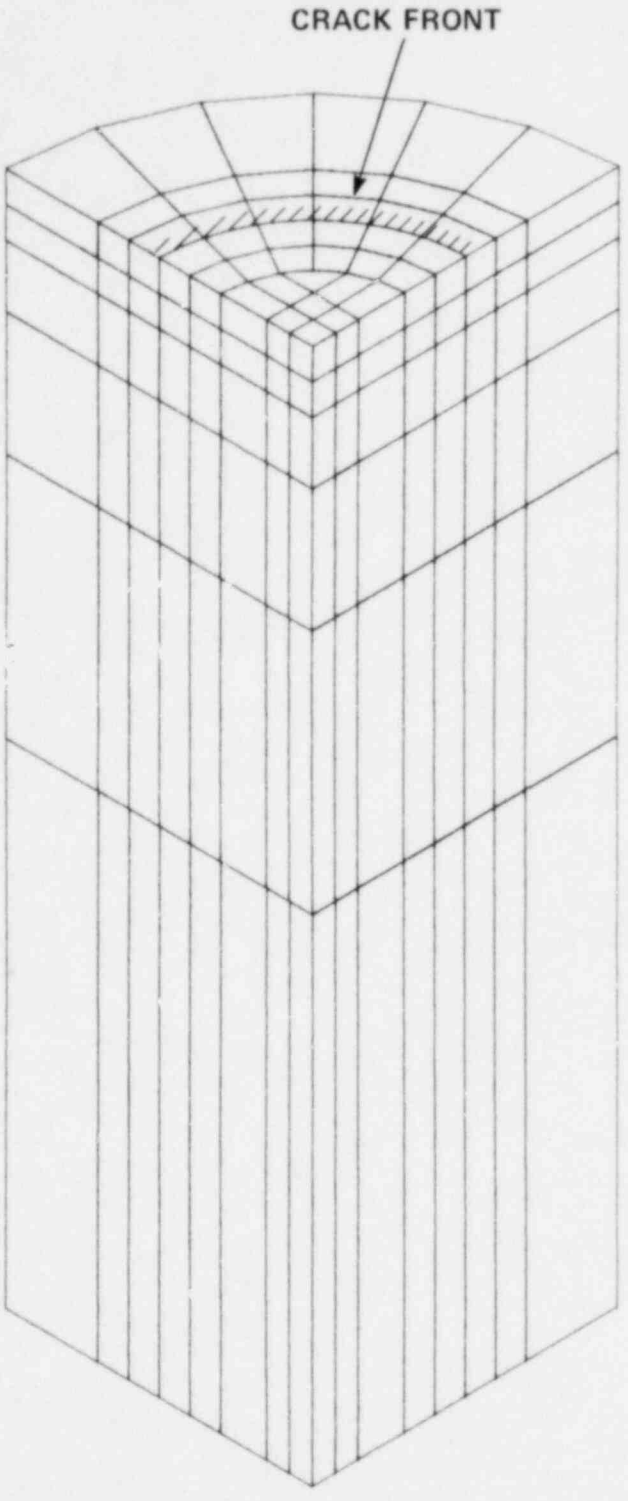

Figure 9. Three-dimensional FE mesh used with the circular crack problem

Table 3

Nodal displacements from FE analysis for a central circular crack in the cylindrical bar with $\nu = 0.25$ (Ratio of crack-to-cylinder radii = 0.5)

Distance r from Crack Tip		Nodal Displacements	
mm	in.	μm	in.
6.35	0.25	18.4	$.724 \times 10^{-3}$
25.4	1	33.3	1.310
38.1	1.5	40.1	1.583
50.8	2	45.0	1.773
69.9	2.75	50.2	1.977
88.9	3.5	53.6	2.112
98.4	3.875	54.8	2.15[illegible]
108	4.25	55.6	2.189
117.5	4.625	56.1	2.208
127	5	56.2	2.214

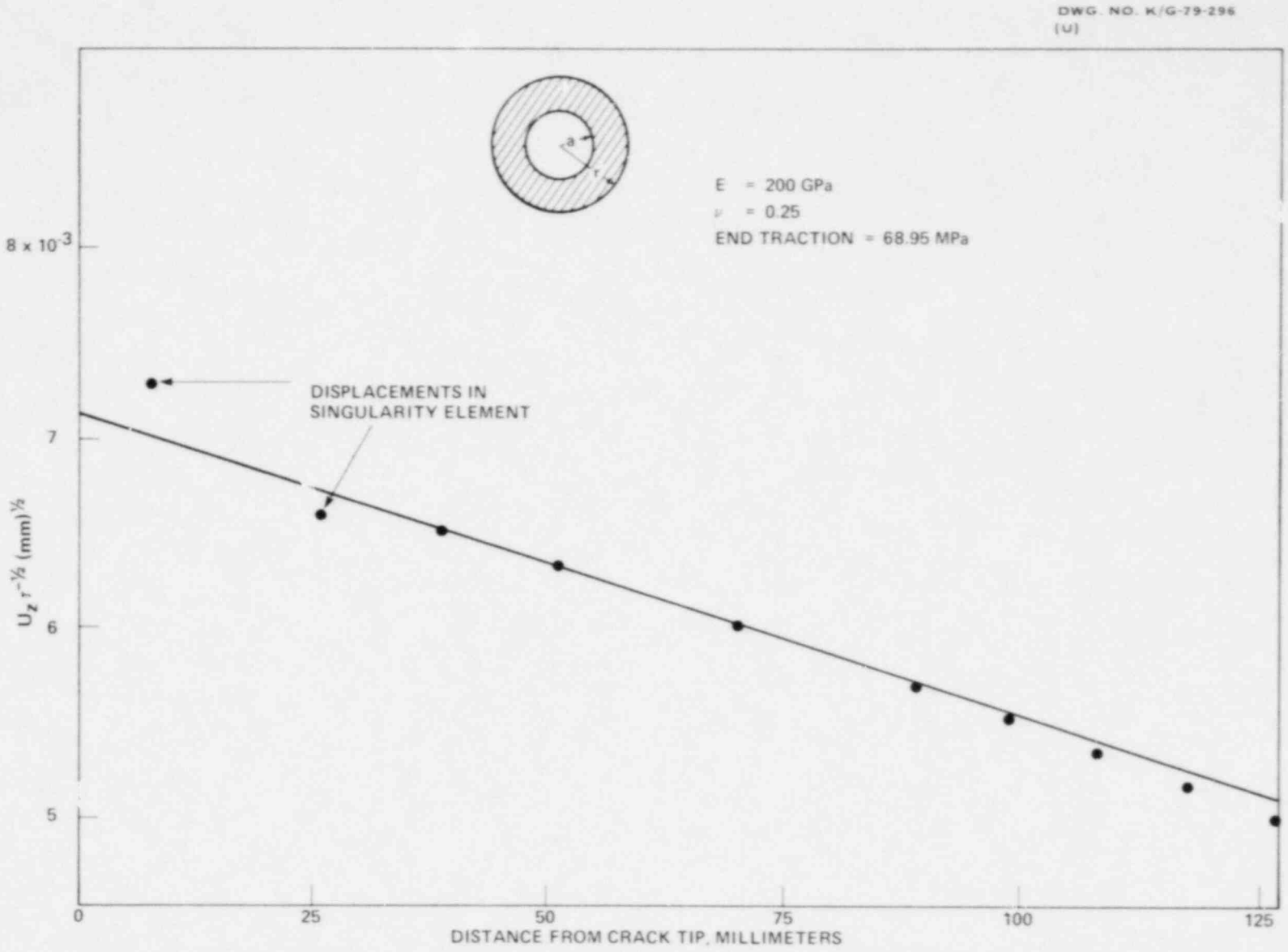

Figure 10. Plot of the $u_z\ r^{-1/2}$ results from the circular crack problem

were performed. The results of the finer mesh were almost identical to those from the coarser one.

3.3.2. Variation of K_I in an Axially Cracked Cylinder Subjected to Thermal Shock (the End Effect Problem)[11]

The object of this series of analyses was the determination of the effect of the free ends on the values of K_I for a specific thermal shock problem. The problem is that of a thick cylinder with an axial crack extending along the whole length, Figure 11(a). As the length of the cylinder increases, the K_I values along a central portion of the crack will approach the 2-D plane strain value. The problem of concern is to determine the minimum lengths that will satisfy a required relationship between the 2-D and 3-D K_I values over a specified central portion of the cylinder.

The cylinder analyzed has an inner radius of 343 mm and a wall thickness of 152 mm. It is initially at a uniform temperature of 129°C. The inside surface is quenched with coolant at -196°C. The thermal analysis was performed on a one-dimensional axisymmetric model using the HEATING5 [23] code with the data shown in Table 4 and some of the resulting temperature distributions through the wall thickness is given in Figure 12. The radial temperature distributions were used in the FE analysis of the cracked cylinder. Figure 11(b) shows the models[12] analyzed while Table 5 gives the cylinder lengths, times in the transient,

---

[11] If the ratio cylinder-length-to-outside-radius is of the same order of magnitude as unity, neither the plane strain nor the plane stress assumptions are useful and complete 3-D theory must be employed [22, p. 289].

[12] Details of the method of mesh generation and profile reduction are given in Appendix A. The 2-D mesh used to generate the 3-D meshes is similar to that shown in Figure 7.

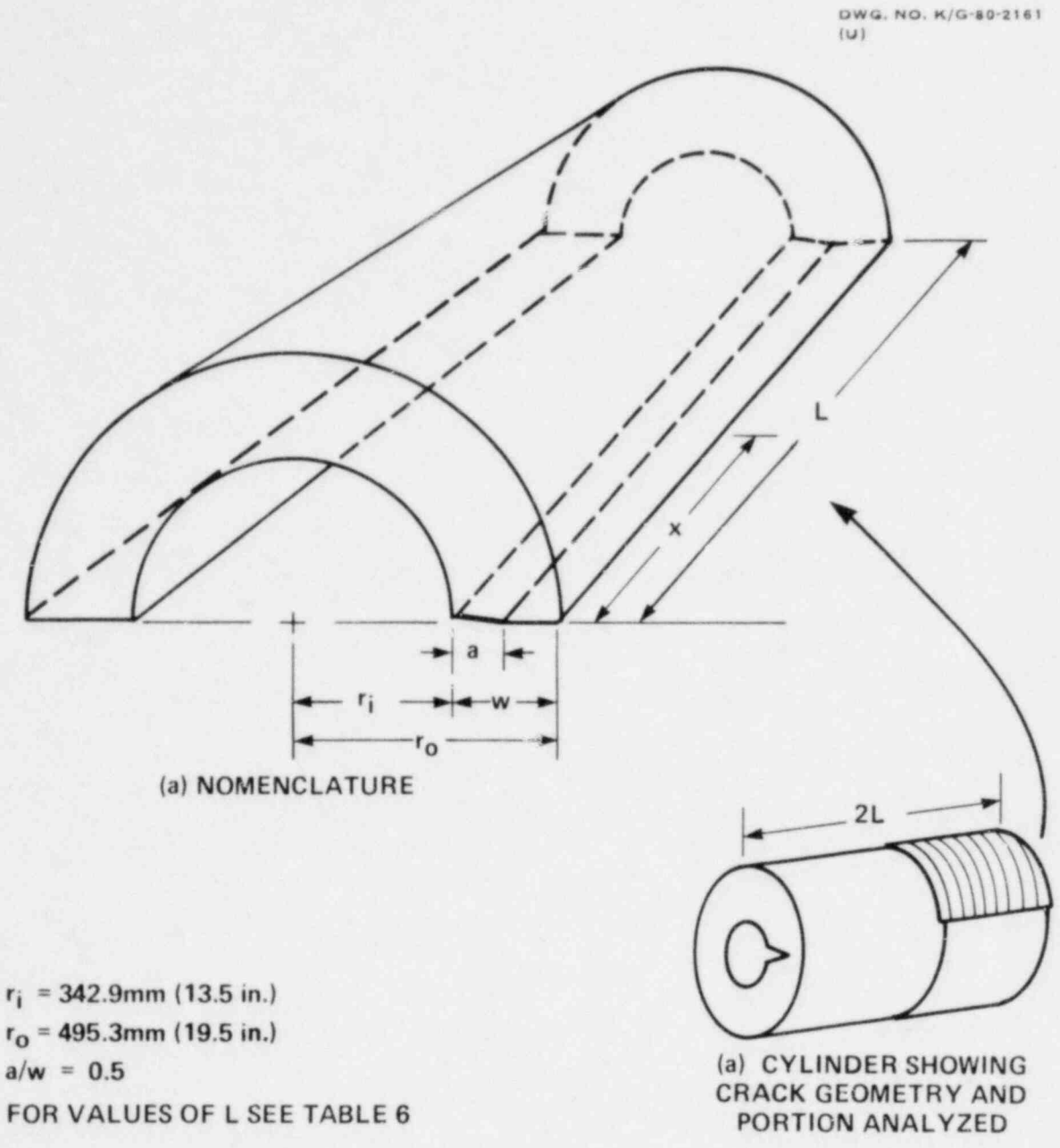

Figure 11. Notation used in the end effects study: (a) geometry of the problem, (b) nomenclature

Table 4

Input data for HEATING5 analysis,
case designation 13C
(One-dimensional axisymmetric solution)

Cylinder Radii	
Inside	343 mm (13.5 in.)
Outside	495 mm (19.5 in.)
Initial Temperature	129 °C (264 °F)
Coolant Temperature	-196 °C (-320 °F)
Density	7·83 g·cm (489 lb. $ft.^{-3}$)
Conductivity	43·3 $W \cdot m^{-1} \cdot K^{-1}$ (25 $Btu \cdot hr^{-1} \cdot ft^{-1} \cdot °F^{-1}$)

Specific Heat[a]

SI		US Units	
°C	$J \cdot Kg^{-1}\ K^{-1}$	°F	$Btu \cdot lb^{-1}\ °F^{-1}$
-184	184	-300	0.044
-157	251	-250	0.060
-129	312	-200	0.0745
-101	356	-150	0.085
- 73	385	-100	0.092
- 46	406	- 50	0.097
- 18	423	0	0.101
38	452	100	0.108
93	479	200	0.1145
149	503	300	0.1202
204	528	400	0.1260
260	551	500	0.1315
316	574	600	0.1370

Table 4 (Contd.)

Surface Heat Transfer Coefficient[a]			
°C[b]	$kW \cdot m^{-2} K^{-1}$	°F[b]	$Btu \cdot hr^{-1} ft^{-2} °F^{-1}$
-176	5.31	-285	936
-162	4.05	-260	714
-148	3.01	-235	530
-134	2.22	-210	391.2
-121	1.64	-185	288
-107	1.21	-160	213.6
- 92.8	0.886	-135	156
- 78.9	0.668	-110	117.6
- 71.9	0.586	- 97.5	103.2
- 65	0.531	- 85	93.6
- 58.1	0.511	- 72.5	90

[a]For temperatures outside this range, the values at the end of the table are used.

[b]These are the film temperatures used by the HEATING5 code, and are the average of the surface temperature and the coolant temperature.

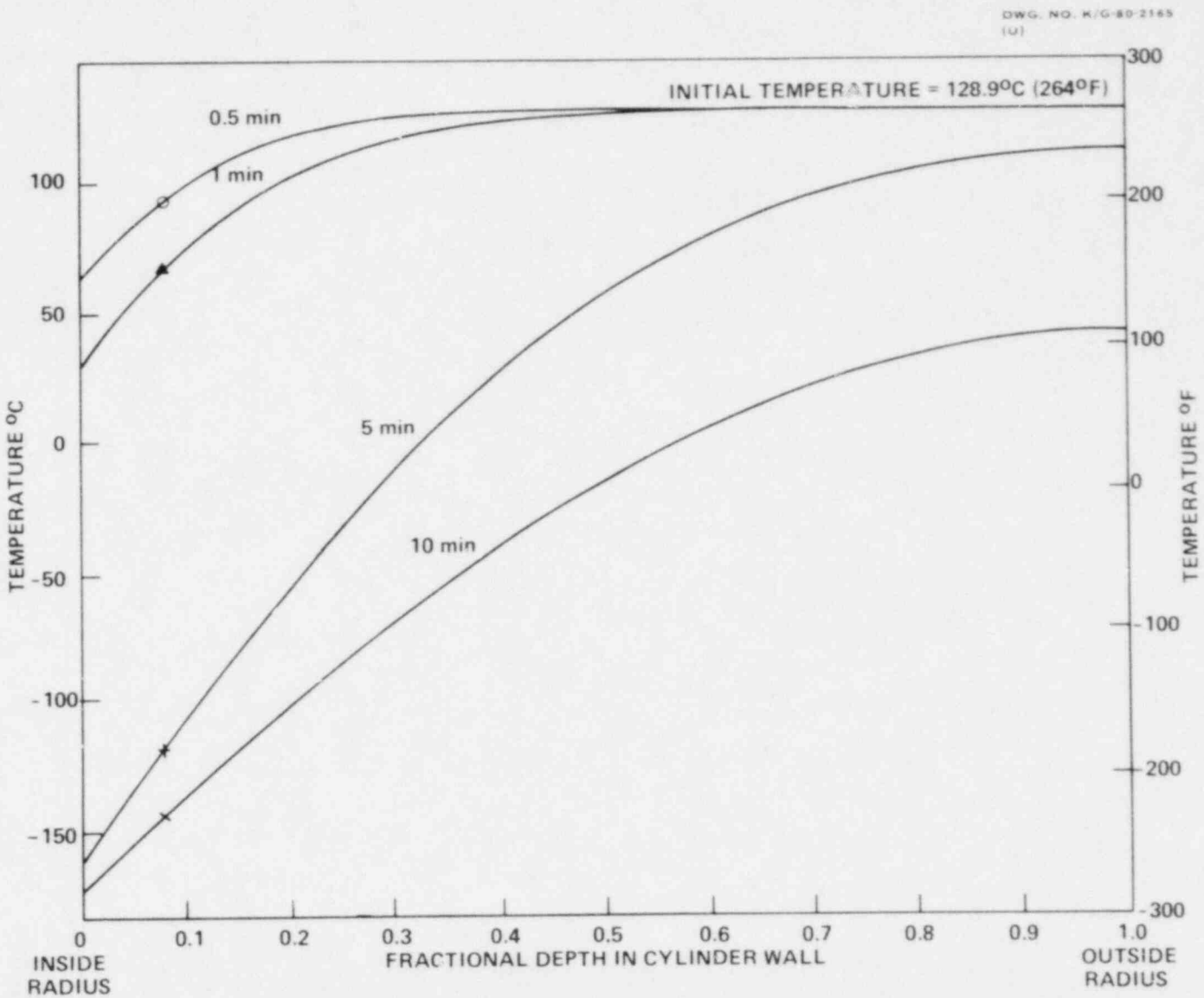

Figure 12. Temperature distributions calculated by HEATING5 and used in the end effects study

Table 5

Data used in the free-end-effects study on cylinders

Temperature distribution designation 13C

Nominal Axial Lengths 2L		Time in Transient
mm	(in.)	minutes
406	(16)	5
686	(27)	5
914	(36)	1, 5, 10
1219	(48)	5

Radii

Inside	343 mm (13.5 in.)
Outside	495 mm (19.5 in.)

Material Properties

Young's modulus	E	193 GPa (28×10^6 psi)
Poisson's ratio	ν	0.3
Coefficient of linear expansion	α	11.7×10^{-6} °C^{-1} (6.5×10^{-6} °F^{-1})
Fractional crack depth	a/w	0.5

	2-D K_I Values MPa·m$^{1/2}$ (ksi·in.$^{1/2}$)			
Time in Transient (Minutes)	0.5	1	5	10
Displacement Method	21.6 (19.7)	37.4 (34.0)	180.2 (164)	149.4 (136)
Strain Energy Method	19.56 (17.8)	38.3 (34.9)	181.2 (164.9)	150.4 (136.9)

the material properties, and the 2-D plane strain K_I values. These K_I values were calculated using both the energy and the displacement methods. The results are very close to each other, an indication of the accuracy of either method.

The results of calculations for 914 mm (36 in.) length and three different times in the transient (1, 5, and 10 minutes) are shown in Figure 13. The 3-D K_I values (K_{I3D}) were normalized by dividing them by the 2-D K_I value (K_{I2D}).

It appears that for this particular problem the end effects are largely independent of the time in the transient. Thus, calculations for other cylinder lengths were made for a single time in the transient.

The results of analyzing different cylinder lengths are shown in Figure 14. The K_I values near the mid-length are all greater than the corresponding 2-D value, except for the very short cylinder. In the shortest cylinders, the K_{I3D} values never attained the K_{I2D} values. For the longer cylinders, the K_{I3D} values exceeded K_{I2D} for some portion of the cylinder length and then dropped rapidly to zero. The percentage of the cylinder length with K_{I3D} values within ± 15% of K_{I2D} was 23%, 47%, 67%, and 73% for the 406, 686, 914, and 1219 mm cylinders.

It may be worth noting that the free ends rotate inwards so that the ends appear to be concave, with the deepest point towards the inside radius (Figure 15). This is, of course, due to the inside being cooler than the outside, which tends to result in closing of the crack near the ends. In the 3-D

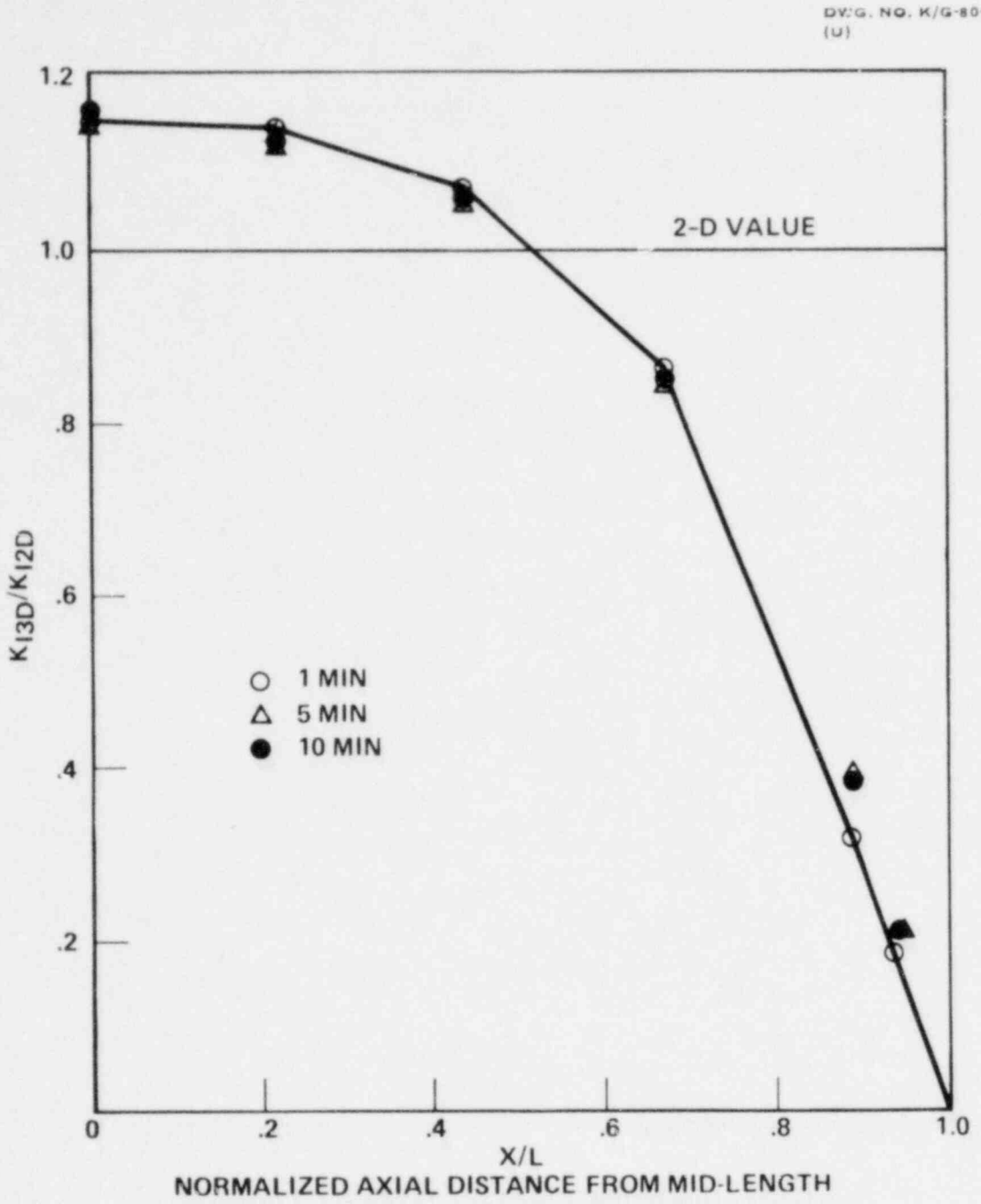

Figure 13. Variation of K_I with distance from mid-length for different times in the transient for the 914 mm (36 in.) cylinder

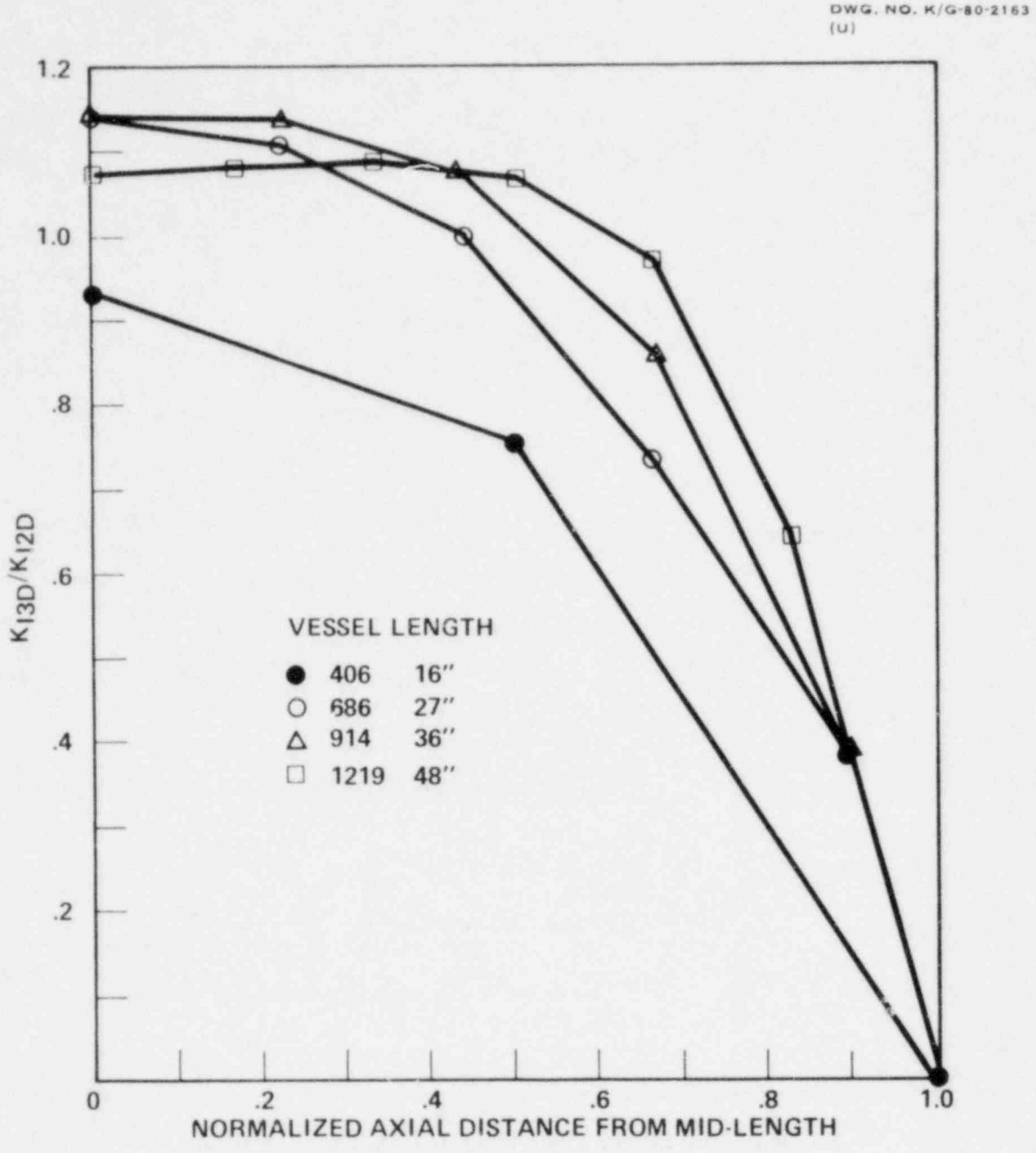

Figure 14. Variation of K_I with axial distance from mid-length for different cylinder lengths

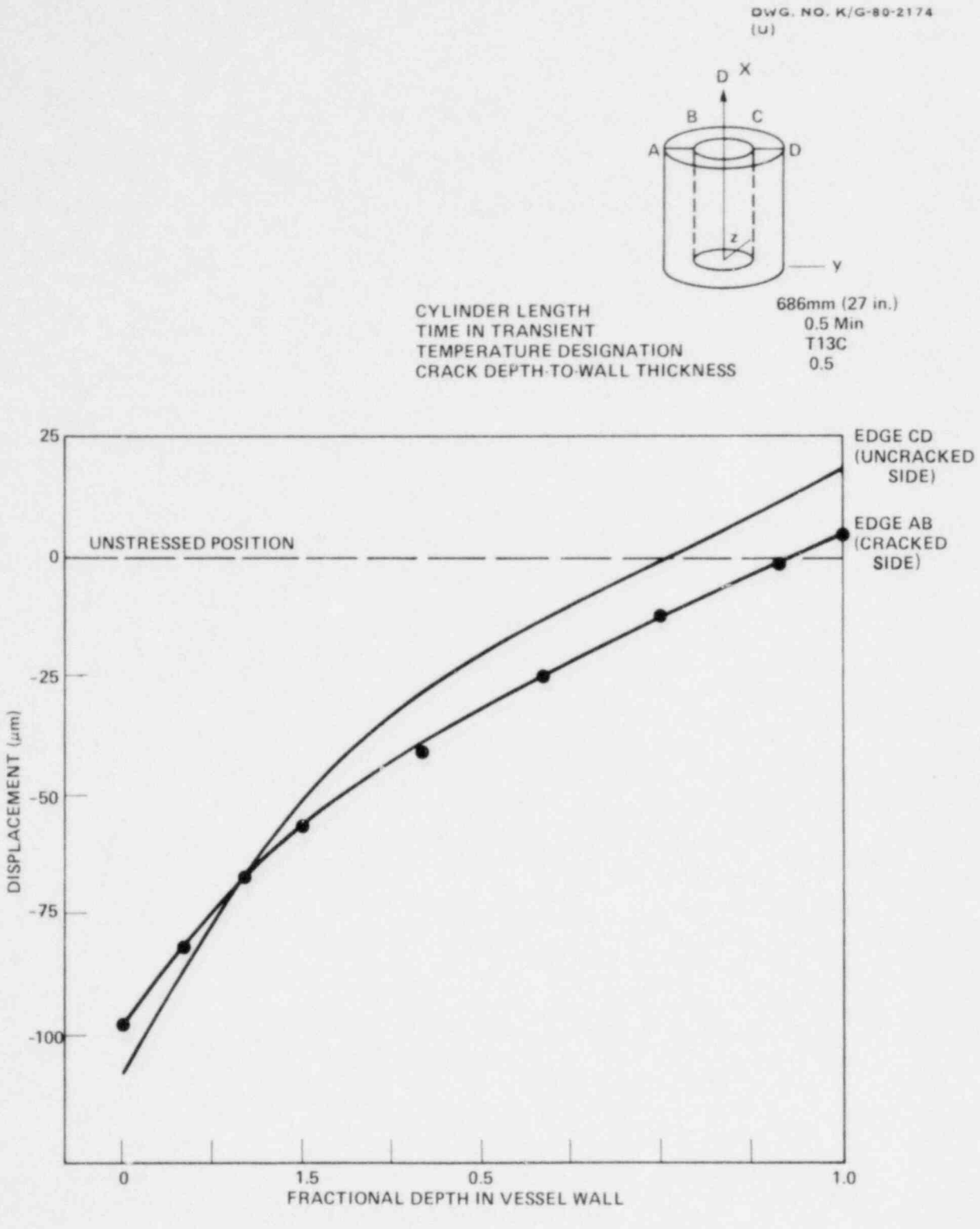

Figure 15. Axial displacements at the free end of radial lines on the plane of symmetry

analysis, the nodes on the crack front were free to move and the two nodes at the end of the cylinder and closest to the crack root moved in such a way as to have "crossed" over the line of symmetry (see Figure 16). Such an anomalous behavior, of course, has no physical reality since the other face of the crack will prevent such an occurrence. This effect can be prevented by the use of crack elements, gap elements, etc. However, a simple stratagem was to fix *a priori* the nodes that had exhibited such a behavior in a previous analysis. This was tried out and had a negligible effect on the K_{I3D} values. The tendency of the nodes at the free ends and closest to the crack tip to close took place in all the cylinder lengths analyzed and, hence, the K_{I3D} values at the free ends were assigned zero values.

3.3.3. Analysis of the V-8 Cylinder

Another example of the 3-D fracture mechanics analysis is that performed on a cylindrical vessel designated as V-8. This vessel was tested in 1979 as a part of the ongoing HSST program, and full details may be found in Reference [24] with a summary in Reference [25]. It consists of an internally pressurized cylinder, closed at the ends, and with an external flaw.

Figure 17 gives the dimensions of the V-8 cylinder and the associated crack as modeled. Symmetry allowed the modeling of only one quarter of the cylinder. As explained in Appendix A, a 2-D mesh is produced from which the 3-D one is generated. Furthermore, the 2-D mesh itself is composed of two separate portions (coarse and fine) that are later merged together, as illustrated in Figure 18.

DWG. NO. K/G-80-2172
(U)

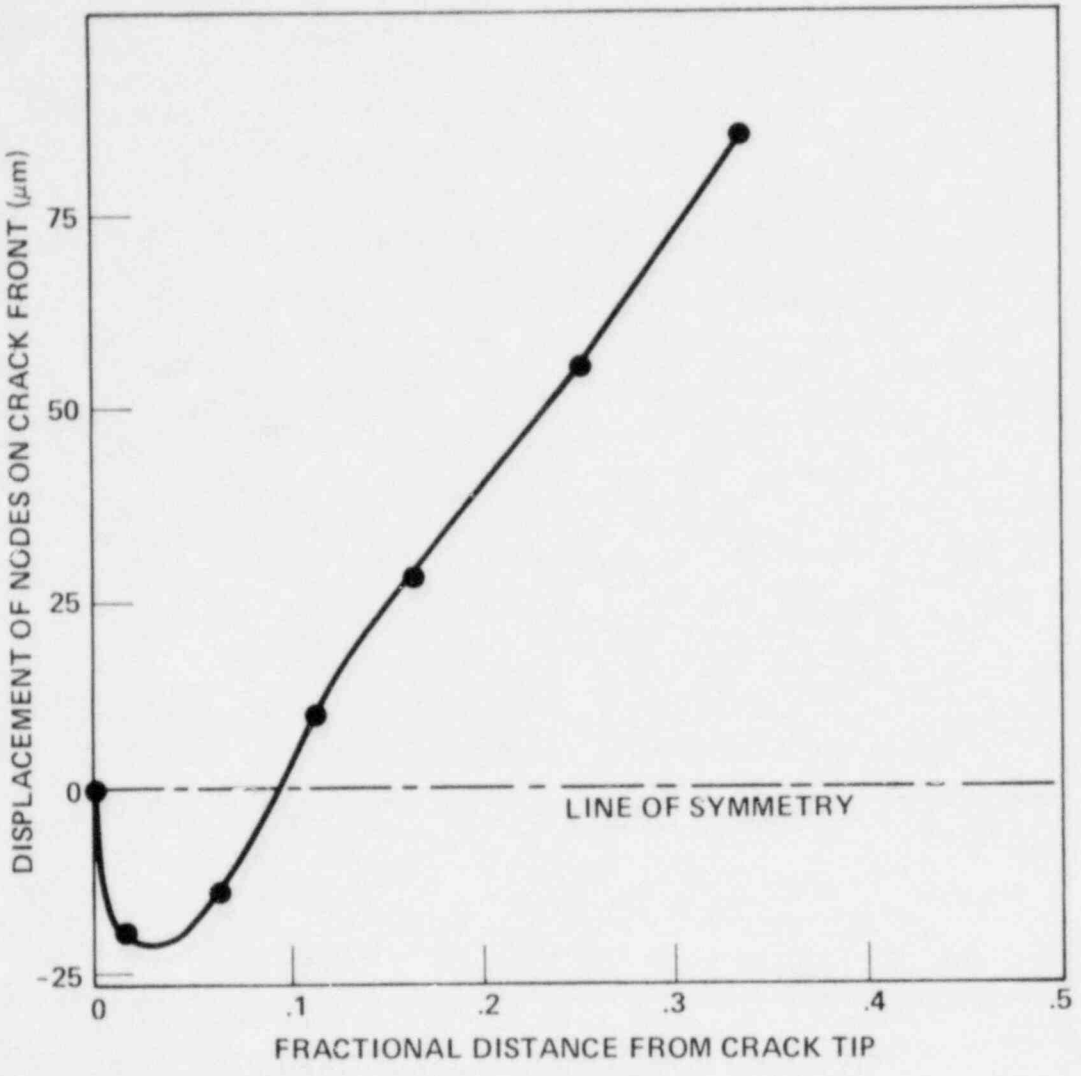

Figure 16. Anomaly in crack opening displacements near the free end

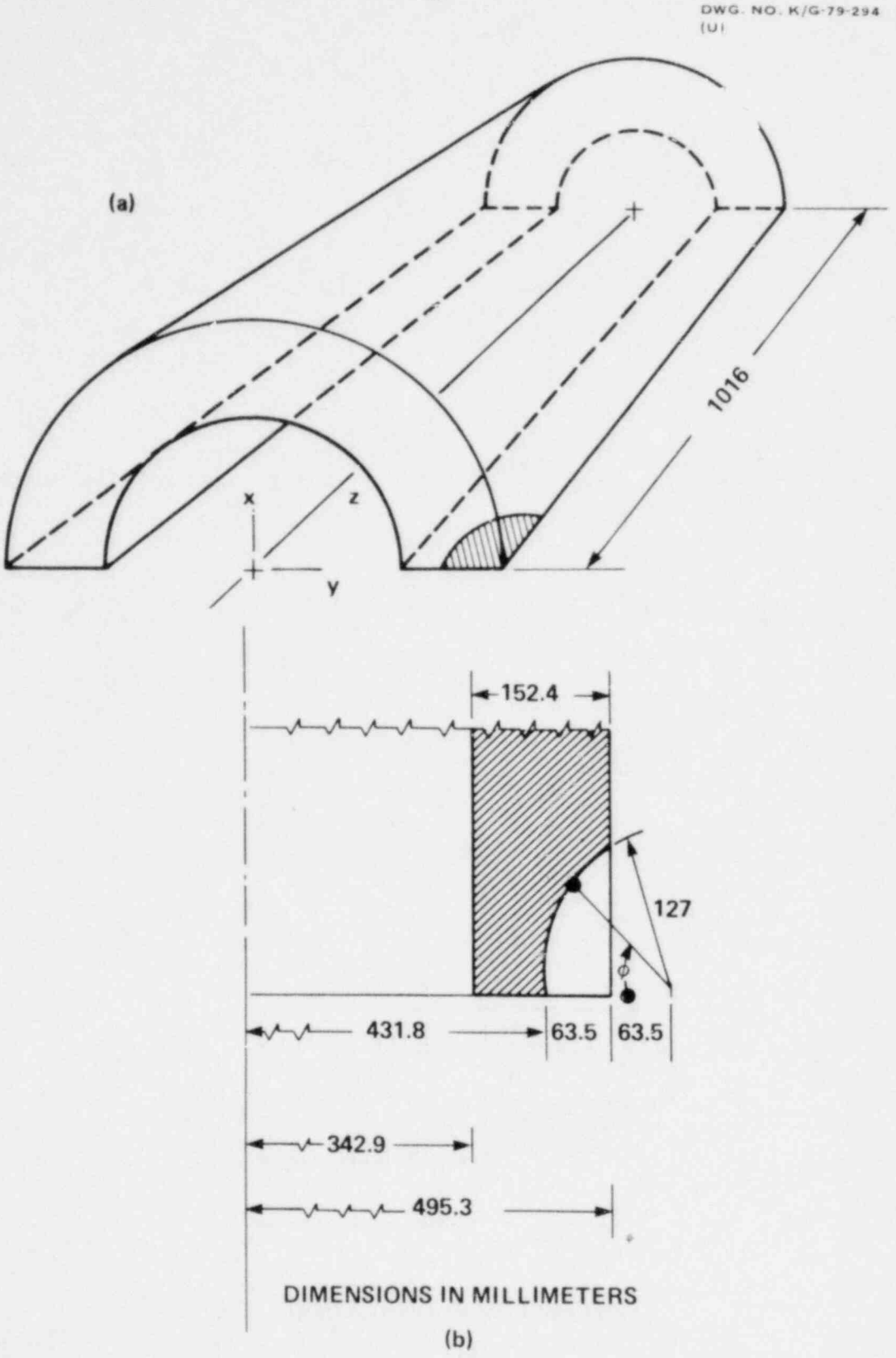

Figure 17. FE model used in the analysis of the V-8 cylinder: (a) quarter cylinder analyzed, (b) crack geometry

DWG. NO. K/G-80-2175
(U)

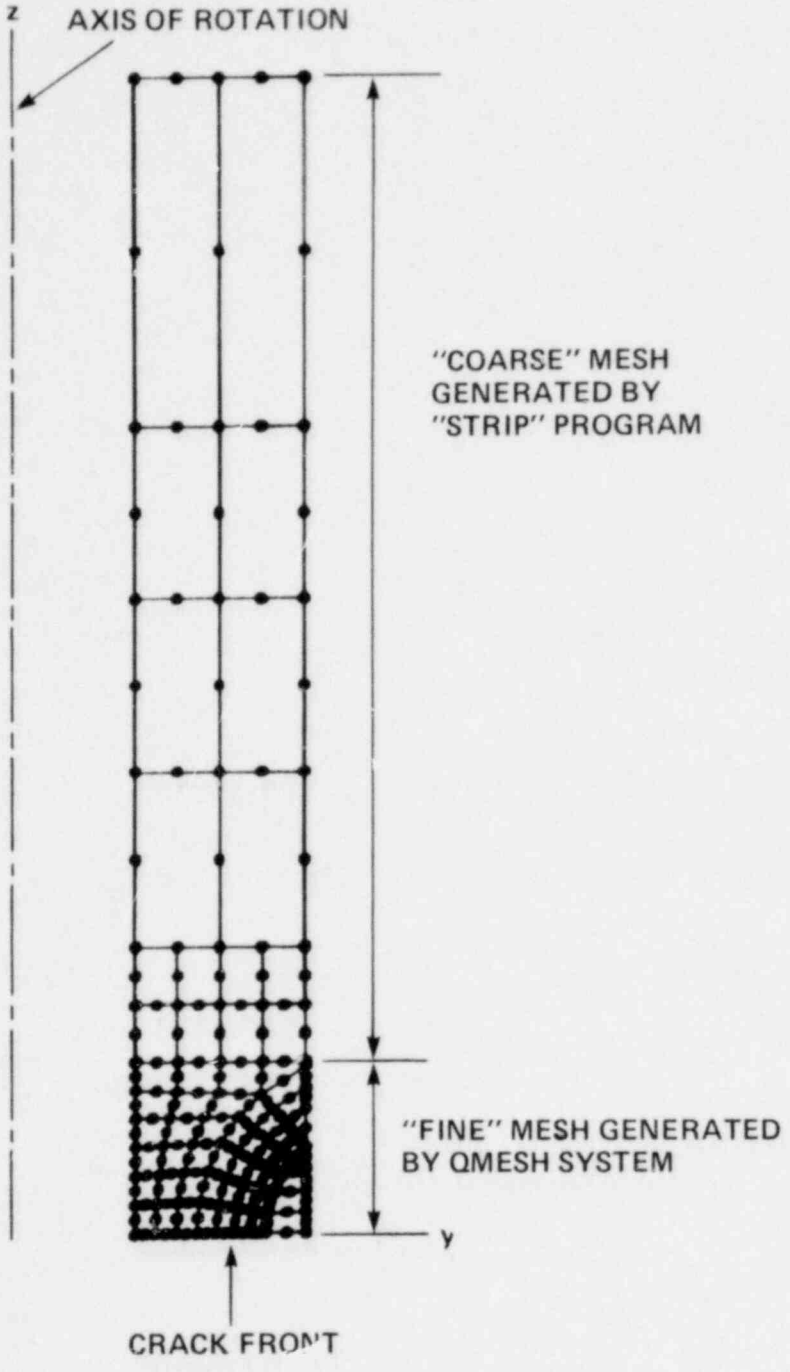

Figure 18. Two-dimensional generating plane for the V-8 cylinder analysis showing the "fine" and "coarse" mesh regions

For the purpose of a convergence study, two FE models were analyzed in which the basic 2-D meshes of the cylinder wall differed in the "fine mesh" region (Figure 18) close to the flaw. The "coarse mesh" portion was the same for both meshes. The 2-D models of the fine mesh region are shown in Figures 19 and 20, and these are designated Mesh 1 and Mesh 2, respectively. Mesh 2 produced about 50% more degrees of freedom (DOF) in the 3-D mesh. The 3-D meshes were generated from these 2-D meshes as described in the Appendix A. Figure 21 illustrates such a 3-D mesh generated from Mesh 1. The angles subtended by the elements in the circumferential direction and used to generate the 3-D meshes, the number of nodes, elements, DOF, etc., together with the computer resources required in the analyses are given in Appendix B.

Under an internal pressure of 69 MPa (10 ksi) the nodal displacement at the outside surface of the cylinder at the center of the crack for Mesh 1 and Mesh 2 were 99.5 μm (3.92×10^{-3} in.) and 99.8 μm (3.93×10^{-3} in.), respectively, a change of about 0.25%. It was concluded that no significant benefit would be realized in analyzing the finer mesh.

The four analyses performed are summarized in Table 6; the resulting displacements normal to both the crack face and the crack front at various angles θ (Figure 17(b)) are given in Table 7. These displacements were used to calculate the K_I values given in Table 8 by means of the displacement method described in Chapter 2. These K_I values were compared to those calculated by other methods [24, Table 4.6]. It appears that the K_I values calculated by the method described above are accurate.

DWG. NO. K/G-80-2167
(U)

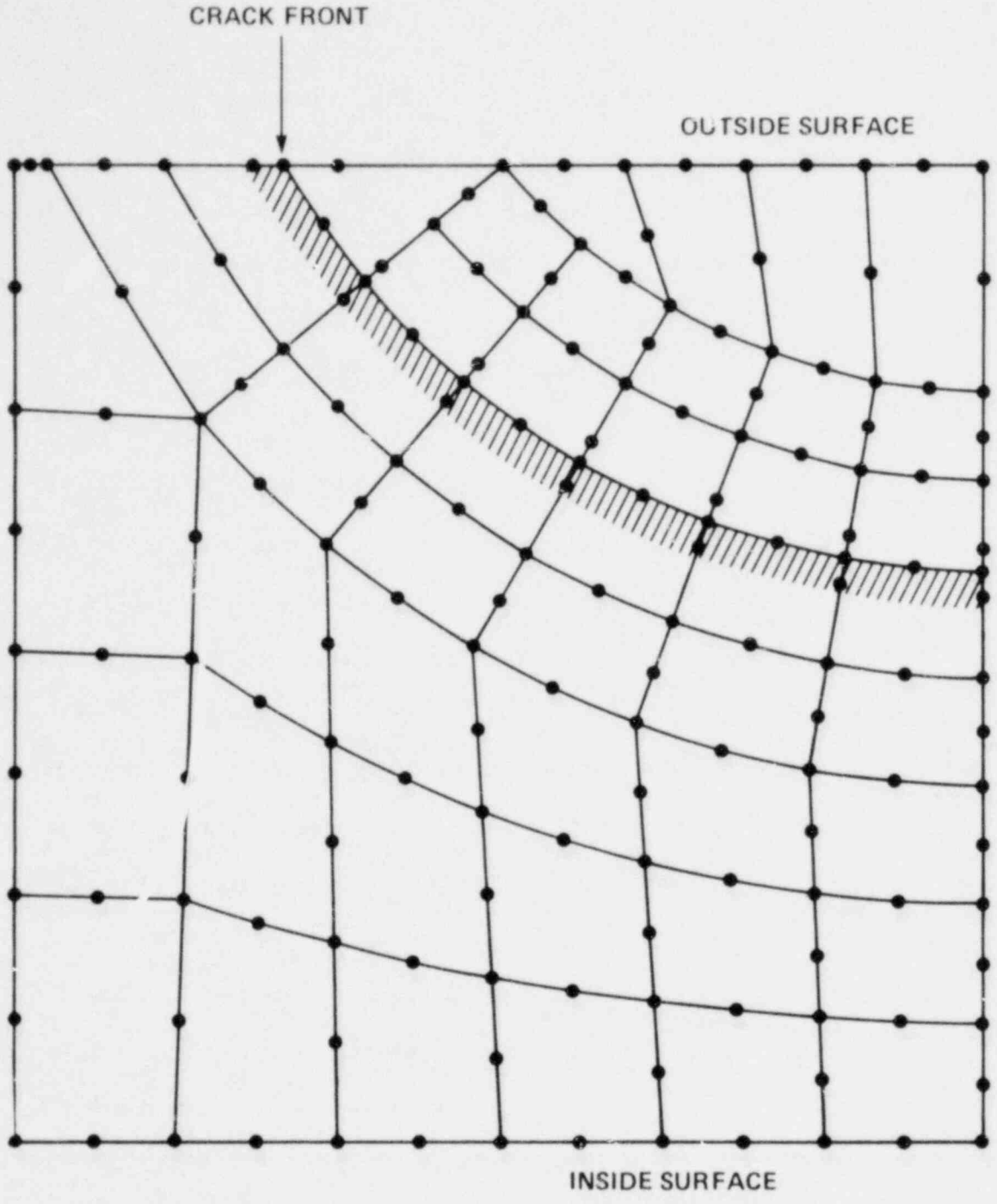

Figure 19. Two-dimensional "fine" mesh portion of the generating plane (Mesh 1) for the V-8 cylinder

DWG. NO. K/G-80-2169
(U)

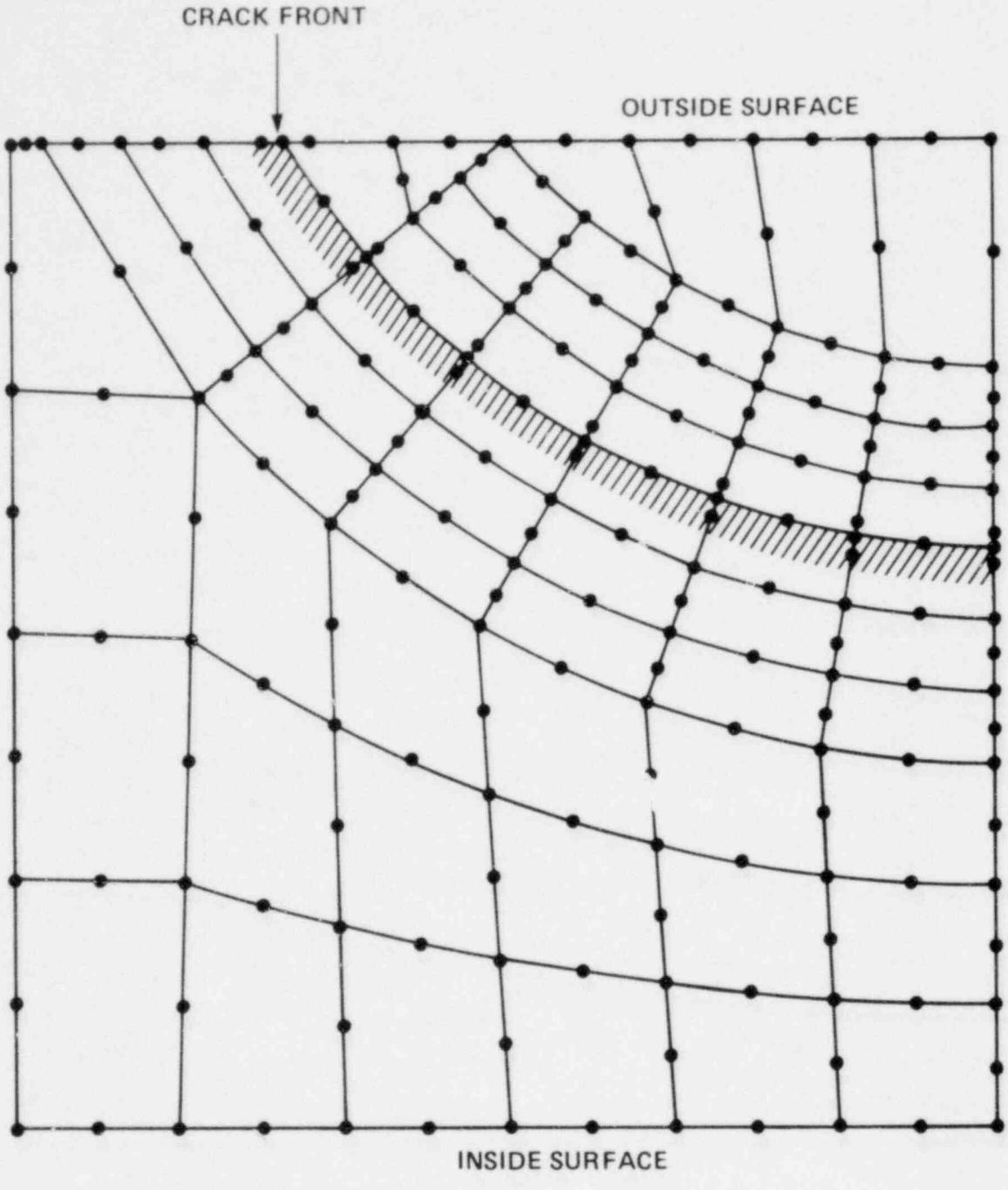

Figure 20. Two-dimensional "fine" mesh portion of the generating plane (Mesh 2) for the V-8 cylinder with more nodes than Mesh 1

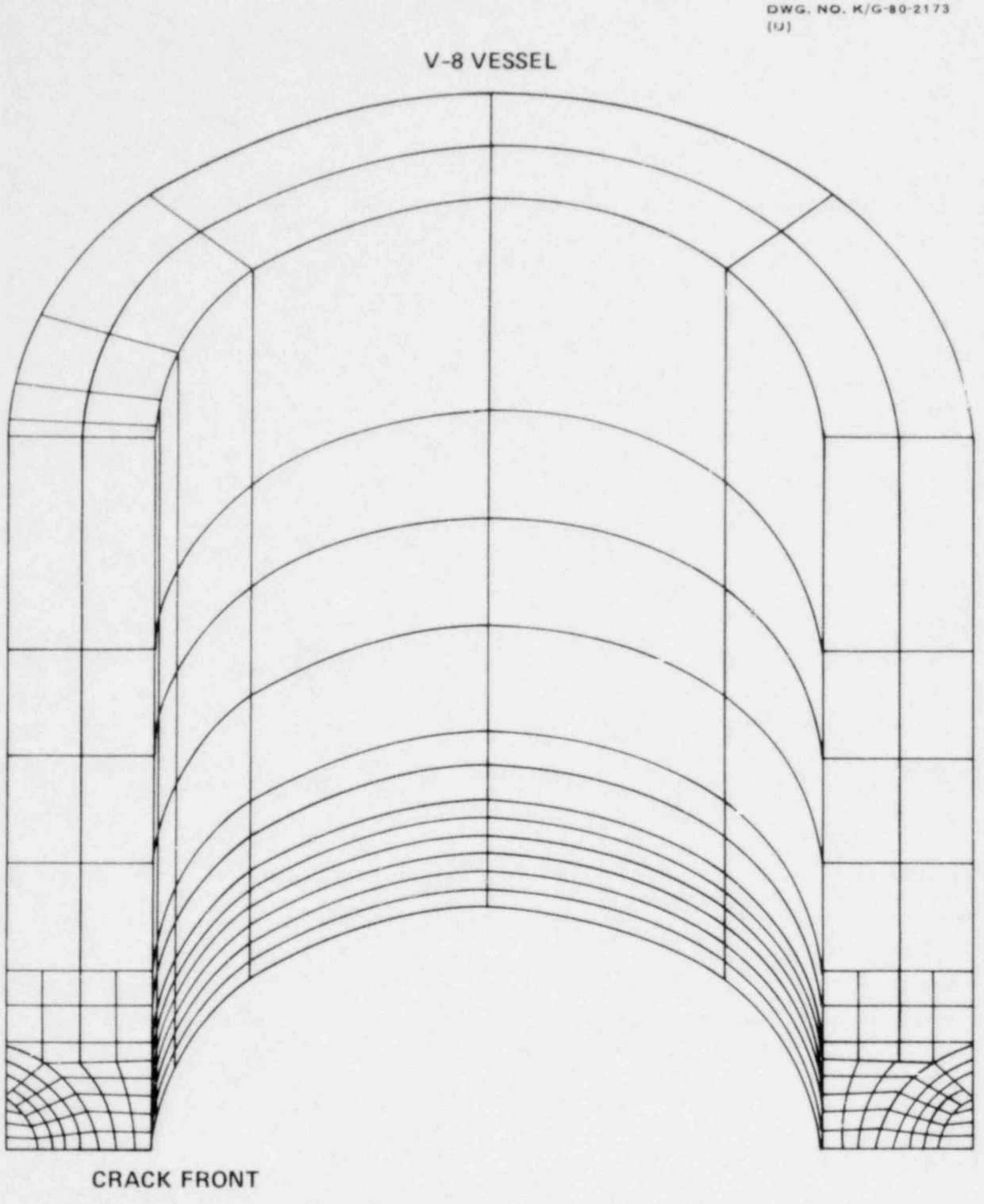

Figure 21. Three-dimensional mesh generated from that shown in Figure 18 for the V-8 cylinder analysis

Table 6

Cases analyzed for V-8 test[a]

Young's Modulus	E = 200 GPa
Poisson's Ratio	ν = 0.29

Case Number	Loading
1	Internal pressure 68.95 MPa
2	Ditto, using finer Mesh No. 2
3	Uniform Pressure on Crack Surface 68.95 MPa
4	Pressure on Crack surface varying linearly from 127.6 MPa at the deepest point in the flaw corresponding to a radius of 431.8 mm to 255 MPa at the outside radius of 495.3

[a]Except for Case 2, these were all performed using Mesh No. 1.

Table 7

Nodal displacements obtained from FE analysis of the V-8 cylinder for the four load cases

Load Case 1
Internal Pressure 68.95 MPa with Mesh No. 1

Node Designation[a]	2	3	4
r mm	14.10	21.15	28.19
Angle ϕ	Nodal Displacements μm		
0	47.22	57.58	65.58
10	47.09	57.45	65.46
20	46.74	57.05	65.13
30	46.08	56.34	64.59
40	45.01	55.22	63.86
50	42.47	52.93	62.89

Load Case 2
Internal Pressure 68.95 MPa and "Finer" Mesh (Mesh No. 2)

Node Designation[a]	2	3	4	5	6
r mm	9.53	14.10	18.80	23.50	28.19
Angle ϕ	Nodal Displacements μm				
0	38.40	47.63	54.58	60.50	65.86
10	38.30	47.47	54.43	60.38	65.74
20	37.95	47.09	54.03	59.99	65.41
30	37.31	46.38	53.31	59.33	64.90
40	36.32	45.24	52.22	58.42	64.24
50	33.99	43.13	50.67	57.48	64.29

Table 7 (Contd.)

Load Case 3
Crack Surface Pressurized with a Uniform Pressure of 68.95 MPa

Node Designation[a]	2	3	4
r mm	14.10	21.15	28.19
Angle ϕ	Nodal Displacements μm		
0	23.61	28.96	33.20
10	23.59	28.93	33.17
20	23.54	28.88	33.15
30	23.40	28.73	33.07
40	23.11	28.42	32.94
50	21.98	27.38	32.54

Load Case 4
Crack Surface Pressurized with a Linearly Varying Pressure,
127.6 MPa at Crack Root and 255.1 MPa at Outer Surface

Node Designation[a]	2	3	4
r mm	14.10	21.15	28.19
Angle ϕ	Nodal Displacements μm		
0	65.13	82.19	97.08
10	65.66	82.78	97.71
20	67.23	84.51	99.52
30	69.55	87.02	102.21
40	72.06	89.79	105.38
50	71.96	90.09	107.49

[a]These node designations are indicated in Figure 3. Displacements at node 1 are inaccurate as mentioned in text.

Table 8

K_I in $MNm^{-3/2}$ as a function of ϕ[a]

	Angle ϕ					
Case Load	0°	10°	20°	30°	40°	50°
1	55.2	55.5	54.9	53.5	52.0	46.4
2	55.7	55.9	55.7	53.7	52.2	47.4
3	48.3	48.3	47.9	47.7	47.5	43.2
4	71.4	71.9	73.8	76.7	80.1	78.2

[a] 60° is the point at the free surface.

4. DISCUSSIONS AND CONCLUSIONS

The energy and stress/displacement methods used to calculate K_I in 2- and 3-D problems have been documented in this report. These methods have been used for solving problems of interest to the HSST program. The stress/displacement methods are based upon the near field equations relating the stresses and displacements to the stress intensity factors. Some approximation is involved in the use of these equations, namely, the higher order terms are neglected since these terms are, in general, unknown. The term used is valid only in the "vicinity" of the crack. It was therefore important to validate the method through the solution of test problems with closed form solutions. The resulting methodology was used successfully for the solution of both 2- and 3-D problems, some of which have been presented in this report.

Energy methods described in this report do not involve such an approximation at the theoretical level. The approximations made are those associated with the numerical methods used and the resulting errors apply to both energy and stress/displacement methods. As such, energy methods are more reliable and accurate than stress/displacement methods. Their main limitation is the practicability of their application to 3-D problems.

This report also discussed the errors that may arise if the strain energy is used in place of the potential energy in problems where both mechanical and thermal loads occur.

Examples of 2- and 3-D problems solved have been presented. For 2-D problems, these have been solved by both energy and displacement methods, and the results of either method compare well with each other.

This indicates that the methods as applied to the type of problems described in this report are accurate and reliable.

One of the errors that may arise in the FE method is that associated with a sufficiently fine mesh, especially in the vicinity of steep stress gradients such as those associated with cracks. Some assurance that an adequately fine mesh was used has been obtained by means of limited convergence studies in which the same problem was solved with two meshes, one of which had more degrees of freedom than the other. No significant change in the results was observed.

The energy methods as implemented in the FMECH code use a four-noded quadrilateral, and the mesh in the crack region is fine enough to allow the depth of the crack to be changed by the small amount ΔA by means of releasing the node at the crack root. This method was preferred to altering the coordinates of crack root node by a small amount to achieve the same purpose because altering the coordinates will distort the two elements sharing that node with a possible loss in accuracy in that region. The stress/displacement method uses an eight-noded 1/4-point element. In terms of computer resources, the eight-noded element is more efficient than a four-noded element. However, the total effort required to compute K_I using the stress/displacement method is more than that required for the energy method since the former requires some manual effort. However, for the 3-D problems the stress/displacement method has proven useful since it is easily implemented if a suitable FE code is available and once the required input data is prepared.

In conclusion, each of the methods discussed in this report have their advantages and limitations, but within these limitations both methods are capable of yielding K_I values within about $\pm 5\%$ accuracy.

REFERENCES

1. Tada, H., P. Paris and G. Irwin, Stress Analysis of Cracks Handbook, Del Research Corp., Providence, Rhode Island, 1973.

2. Besuner, P. M. and W. R. Caughey, "Comparison of Finite Element and Influence Function Methods for Three-Dimensional Elastic Analysis of Boiling Water Reactor Feedwater Nozzle Cracks," NP-261, Electric Power Research Institute, November 1976.

3. Cruse, T. A. and W. VanBuren, "Three-Dimensional Elastic Stress Analysis of a Fractured Specimen with an Edge Crack," Int. J. Fract. Mech., Vol. 7, No. 1, March 1971.

4. Zienkiewicz, O. C., The Finite Element, 3 Ed., McGraw-Hill, 1977.

5. Griffith, A. A., "The Phenomena of Rupture and Flow in Solids," Phil. Trans. Royal Soc. of London, Vol. 221, 1921, pp. 163-198.

6. Irwin, G. R. and J. Kies, "Fracturing and Fracture Dynamics," Welding Jour. Res. Suppl., Vol. 31, 1952, pp. 95s-100s.

7. Orowan, F., "Fundamentals of Brittle Behavior of Metals," Fatigue and Fracture of Metals, John Wiley & Sons, 1952, pp. 139-167.

8. Irwin, G. R., "Analysis of Stress and Strains Near the End of a Crack Traversing a Plate," J. Appl. Mech., Vol. 24, 1957, pp. 361-364.

9. Iskander, S. K., "The Calculation of Stress Intensity Factors in Thick Cylinders Subjected to Transient Temperature Gradients by the Finite Element Method," K/CSD/TM-2, Union Carbide Corporation, Nuclear Division, Oak Ridge, Tennessee, 1976.

10. Hellen, T. K., "On the Method of Virtual Crack Extensions," Int. J. Num. Meth. Eng., Vol. 9, 1975, pp. 187-207.

11. Sokolnikoff, I. S., Mathematical Theory of Elasticity, 2nd Ed., McGraw-Hill, 1956.

12. Kobayashi, A. S., Experimental Techniques in Fracture Mechanics, Society for Experimental Stress Analysis, 1973, Chapter 2, "Fracture Mechanics."

13. Wilkinson, J. H., The Algebraic Eigenvalue Problem, Oxford University Press, 1965.

14. Shah, R. C. and A. S. Kobayashi, "On the Parabolic Crack in an Elastic Solid," Eng. Fract. Mech., Vol. 1, 1968, pp. 309-325.

15. Barsoum, R. S., "On the Use of Isoparametric Finite Elements in Linear Fracture Mechanics," Int. J. Num. Meth. Eng., Vol. 10, 1976, pp. 25-37.

16. Henshell, R. D. and K. G. Shaw, "Crack Tip Finite Elements are Unnecessary," Int. J. Num. Meth. Eng., Vol. 9, 1975, pp. 495-507.

17. Isida, M., "Effect of Width and Length on Stress Intensity Factors of Internally Cracked Plates Under Various Boundary Conditions," Int. J. Fract. Mech., Vol. 7, 1971, pp. 301-316.

18. Bathe, Klaus-Jurgen, "ADINA — A Finite Element Program for Automatic Dynamic Incremental Nonlinear Analysis," Report 82448-1, Acoustics and Vibration Laboratory, Mechanical Engineering Department, MIT, Cambridge, Massachusetts.

19. Cheverton, R. D. and S. E. Bolt, "Pressure Vessel Fracture Studies Pertaining to a PWR LOCA-ECC Thermal Shock: Experiments TSE-3 and TSE-4 and Update of TSE-1 and TSE-2 Analysis," ORNL/NUREG-22, Oak Ridge National Laboratory, Oak Ridge, Tennessee, December 1977.

20. Sneddon, I. N. and J. T. Welch, "A Note on the Distribution of Stresses in a Cylinder Containing a Penny-Shaped Crack," Int. J. Eng. Sci., Vol. 1, 1963, pp. 411-419.

21. Rooke, D. P., Compendium of Stress Intensity Factors, H. M. Stationery Off., London, 1976.

22. Boley, B. A. and J. H. Weiner, Theory of Thermal Stresses, John Wiley & Sons, 1967.

23. Turner, W. D., et al. "HEATING5 — An IBM 360 Heat Conduction Program," ORNL/CSD/TM-15, Oak Ridge National Laboratory, Oak Ridge, Tennessee, 1977.

24. Bryan, R. H., et al., "Test of 6-in. Thick Pressure Vessels, Series 3: Intermediate Test Vessel V-8," ORNL/NUREG-58, Oak Ridge National Laboratory, Oak Ridge, Tennessee, December 1979.

25. Bryan, R. H., et al., "Test of Thick Vessel with a Flaw in Residual Stress Field," 79-PVP-29, ASME PVP Conference, San Francisco, California, June 25-29, 1979.

26. Iskander, S. K., "A Two-Dimensional Plotting Code and Some Useful Two- and Three-Dimensional Mesh Generation Programs for Isoparametric Finite Elements," in preparation.

27. Jones, R. E., "QMESH: A Self-Organizing Mesh Generation Program," SLA-73-1088, Sandia Laboratories, Albuquerque, New Mexico, July 1974.

28. Gibbs, N. E., W. G. Poole, Jr. and P. K. Stockmeyer, "An Algorithm for Reducing the Bandwidth and Profile of a Sparse Matrix," SIAM J. Numer. Anal., Vol. 13, No. 2, April 1976.

29. Hellen, T. K., "Numerical Integration Considerations in Two and Three Dimensional Isoparametric Finite Elements," The Mathematics of Finite Elements and Applications II MAFELAP 1975, Academic Press, 1976.

30. Hellen, T. K., "On Special Isoparametric Elements for Lirear Elastic Fracture Mechanics," Inst. J. for Num. Meth. in Eng., Vol. 11, No. 1.

31. Chan, S. K., I. S. Tuba and W. K. Wilson, "On the Finite Element Method in Linear Fracture Mechanics," Eng. Fract. Mech., Vol. 2, 1970, pp. 1-17.

APPENDICES

APPENDIX A

FINITE ELEMENT MESH GENERATION AND PROFILE REDUCTION

1. Mesh Generation

One important task (in fact, one of the most time-consuming ones in FE modeling) is that of mesh generation. A large number of codes were written, others acquired and implemented, to facilitate this task.

For the cases described in this report, the geometry of the problem allows 3-D meshes to be generated from 2-D ones. By rotating the 2-D mesh, such as that shown in Figure 18 about an axis lying in its plane, a 3-D one may be obtained (Figure 21). Similarly, by propagating a 2-D one, such as that shown in Figure 8, in a direction normal to its plane, the 3-D mesh shown in Figure 9 is produced.

The mesh generating effort may be conveniently divided into two tasks. The first will be termed the "2-D level" and consists of generating the 2-D mesh. The second task, the "3-D level" one, comprises taking the 2-D mesh and producing from it the 3-D mesh.

At the 2-D level, the most important task was the coding of a mesh plotting program and implementing it on the time-sharing PDP-10 system [26]. All the 2-D plots shown in this report were produced by this package. It is capable of plotting the whole structure or, by means of user-defined coordinate limits, it can plot certain areas of the mesh thereby "zooming" on detailed areas. The node and element numbers may be displayed or suppressed.

This allows the analyst to generate and view the mesh. If it is deemed unsatisfactory, the whole process may be repeated. A satisfactory

mesh may be produced in less than an hour. A similar process, when attempted in a batch mode, would take several days to complete.

Generation of the 2-D models of cylinders is accomplished by means of the GEN8 code [26], producing semicircular annuli similar to that shown in Figure A.1(a). The number of elements in the radial and circumferential directions, geometric progression factors for both these directions, and the inside and outside radii are the input parameters.

Strips such as that shown in Figure A.2 have been useful in the modeling process. The centrally cracked strip and the coarse mesh portion of the V-8 cylinder model (both mentioned earlier in this report) as well as many others have been generated by the "STRIP" code [26]. This allows the user to define the number of elements horizontally and vertically as well as their dimensions. The number of horizontal elements may be doubled in number as the mesh is generated vertically down, with a one-time transition from four to five elements possible. This allows a mesh to be produced that can be made finer in regions of high stress gradients.

A third code "MERGE" [26] swaps any two elements designated by the user with a so-called singularity block (Figure A.1(b) and A.2(b)) to produce automatically the 1/4-point singularity elements surrounding the crack tip (Figures A.1(c) and A.2(c)).

The "QMESH" system [27], a very useful tool that generates more complex 2-D meshes, was implemented and used to generate the meshes used, for example, in the centrally cracked circular bar and the V-8 cylinder. Being a general-purpose package, it is, however, too unwieldy to use for simple meshes such as those mentioned above and local mesh refinements are difficult to accomplish.

DWG. NO. K/G-80-2168
(U)

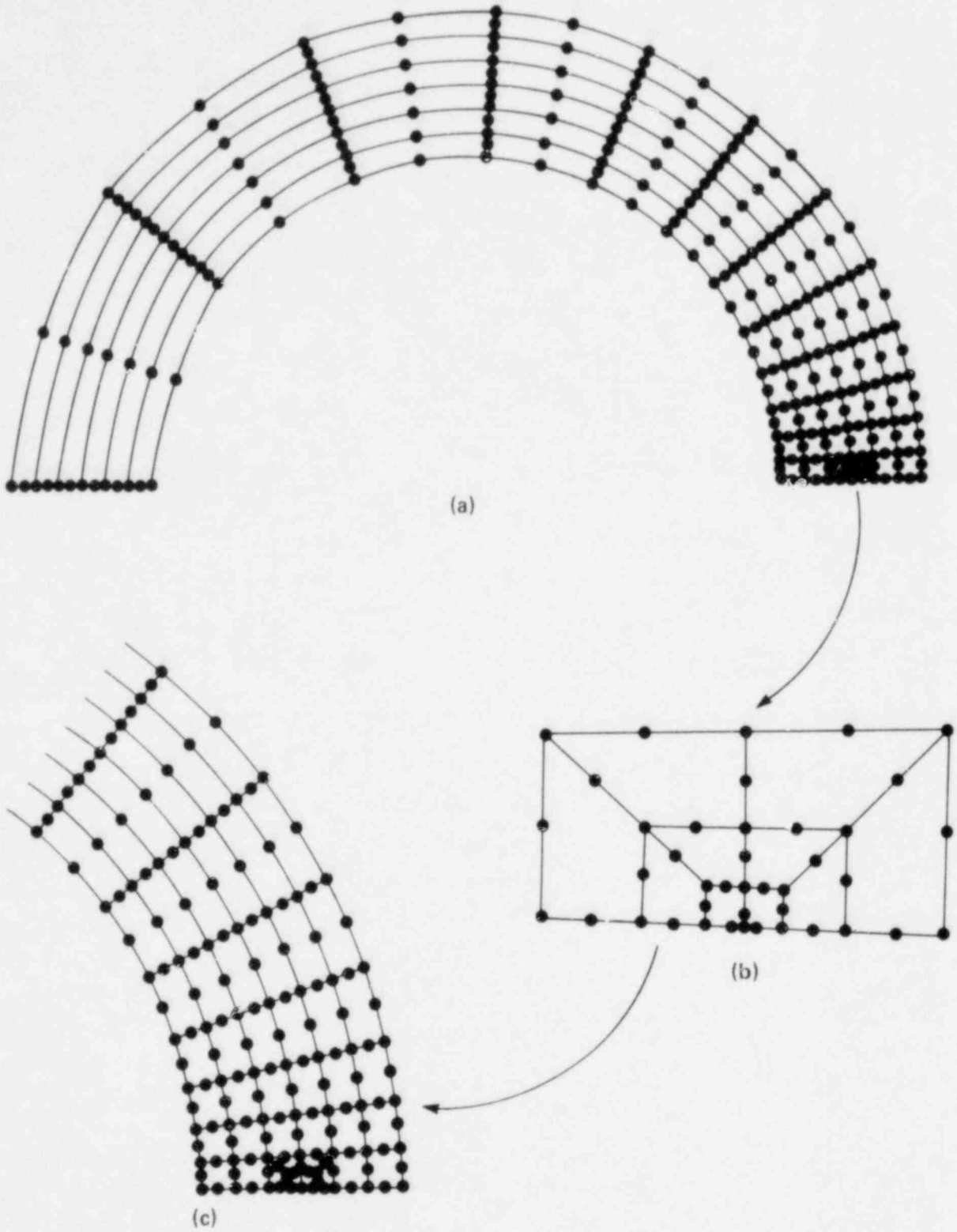

Figure A.1. (a) Typical finite element mesh generated by the "GEN8" code. The singularity block (b) is then "merged" into a pair of elements, e.g., those shown shaded in (a) to produce a model with a "crack" located at a/w = 0.5, a portion of which is shown in (c)

DWG. NO. K/G-80-2170
(U)

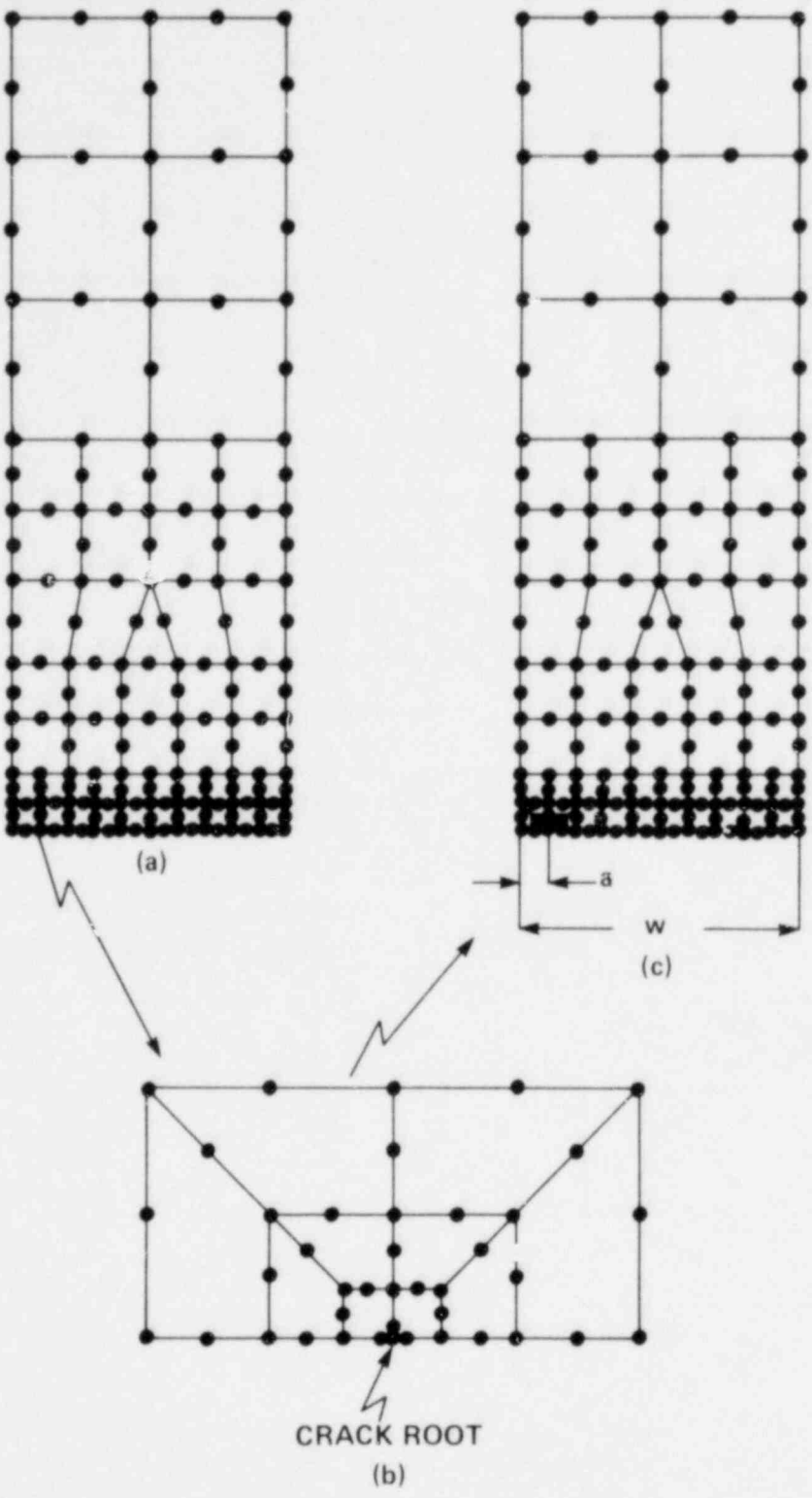

Figure A.2. (a) Example of type of mesh produced by STRIP code, and the incorporation of the singularity block (b) by the MERGE code to produce the mesh (c) used in numerical experiments on the center cracked or edge notched bars. Note that the singularity block can be relocated at different positions giving in this case nine "specimens" with a/w = 0.1 through a/w = 0.9

The generation of 3-D meshes from any of the above 2-D meshes is accomplished by means of the 3-D and V-8 codes [26]. These codes also produce output that allows the user to relate the 3-D models to the 2-D ones. It also produces output identifying element faces in a particular area, if desired. Such output would be useful in the FE analysis of pressure loaded structures, e.g., the V-8 cylinder analysis mentioned in Chapter 3.

The concept of the subdivision of a major task into smaller ones has allowed a considerable amount of modularity in coding the various programs. Furthermore, it permits the user to monitor the satisfactory completion of one task before proceeding to the next one. A major drawback of the 3-D mesh generation codes described above is that *the whole mesh is penalized* by the presence, at the 2-D level, of the fine mesh in the crack region which is then propagated into the third dimension. It is more efficient to implement a merging scheme at the 3-D level similar to that shown in Figures A.1 and A.2 for 2-D meshes. For 3-D meshes, the process is accomplished in three steps. The first consists of generating a relatively coarse mesh for the 3-D structure to be analyzed. Then, a "block" containing the finer mesh required to adequately model the crack region is generated. The final stage would be to merge this block into the mesh for the 3-D structure.

2. Profile Reduction

The bandwidth of automatically generated meshes is, generally speaking, larger than necessary. This condition not only leads to uneconomical FE analyses but, in some instances, to cases impossible

to run on the computer. This is caused primarily by the very high number of input/output (I/O) operations necessary to store and solve out-of-core the large system of linear equations occurring in the FE method of analysis. This, in turn, causes large wall clock times (WCT) during which large segments of memory (1750K) are tied up for say, 10 hours, and unacceptable amounts of scratch disk space are required. Thus, it is imperative to optimize the node numbering scheme. This is accomplished by means of the computer code "REDUCE" [28].

As an illustration of some of the computer resources saved by optimizing the node numbering scheme of the FE models, some pertinent numbers from two separate analyses are given in Tables A.1 and A.2. The problem analyzed is the circular crack described earlier in this report. The "before" refers to values associated with the meshes as generated (i.e., with unoptimized meshes) while the "after" are values associated with the optimized meshes. The figures were compiled from the data generated by the ADINA and the REDUCE codes. These figures show a reduction of 20% to 47% in the computer resources required. The example problem selected was a small one. In cases like that of Mesh 2 of the V-8 analysis, the savings were significant enough to have made the difference between the feasibility or nonfeasibility of the FE analysis.

Table A.1

Effect of node renumbering on the IBM 360/195
computer resources required by
the ADINA computer code
(Approx. 1700K memory used)[a]

Number of Nodes 1286
Number of Elements 234

	Before	After	% Reduction
Number of Matrix Elements (approx.)	1.897×10^6	1.498×10^6	21
Maximum Half-Bandwidth	1415	962	32
Mean Half-Bandwidth	552	436	21
Number of Blocks	29	23	21
CPU Minutes	14	9	36
I/O in Thousands	39	28	28
Wall Clock Time[b] (Minutes)	70	37	47
Approximate Cost[c]	$87	$58	33

[a]Plane Circular Crack problem.

[b]On the IBM 360/195 MVT environment, this can vary widely.

[c]Printed output to tape.

Table A.2

REDUCE code data

	Half-Bandwidth			Profile (approx.)[a]			CPU	Cost[b]
	Before	After	%	Before	After	%	Min	$
Circular Crack	506	331	35	256,000	193,000	25	6	28
Mesh No. 1[c]	1270	626	51	653,000	392,000	40	6	44
Mesh No. 2	1656	593	64	1,278,000	777,000	39	24	115

[a]Profile is the sum of the number of terms in the so-called "sky-line", based on the element connectivity, not upon the actual number of DOF.

[b]Includes print cost.

[c]IBM FORTRAN EXTENDED PLUS compiler generated object code.

APPENDIX B

DETAILS OF THE FE MODELING AND ANALYSIS

In this appendix, details of the FE modeling and analysis are given. Apart from documenting the data used in the 3-D analyses described in Chapter 3, this information has proven useful as a basis for estimating the computer resources required for other similar 3-D computations. This information is important since an upper-limit estimate of the computer resources required in a particular run must be declared before the run is made.

Table B.1

Data used to propagate meshes from 2-D into 3-D

Analysis	Propagation	No. of Elements in 3rd Dimension	Element Thickness or Angular Dimension	Total
Circular Crack	Axial	6	25.4, 25.4, 50.8, 101.6, 203, 406 mm	813 mm.
			(1, 1, 2, 4, 8, 16 in.)	(32 in.)
End Effects Cylinders	Axial			
Nominal Lengths 2L mm (in.)				
406 (16)		2	2 x 101.6 mm (2 x 4 in.)	203 mm (8 in.)
686 (27)		6	3 x 76.2 mm + 3 x 38.1 mm (3 x 3 in. + 3 x 1.5 in.)	343 mm (13.5 in.)
914 (36)		6	4 x 101.6 mm x 2 x 25.4 mm (4 x 4 in. + 2 x 1 in.)	457 mm (18 in.)
1219 (48)		6	6 x 101.6 mm (6 x 4 in.)	610 mm (24 in.)
V-8 Cylinder	Circumferential			
Mesh No. 1		7	3°, 6°, 12°, 24°, 3 x 45°	180°
Mesh No. 2		9	1°, 2°, 4°, 6°, 10°, 22°, 3 x 45°	180°

Table B.2

Miscellaneous data of interest related to the 3-D FE analysis using the ADINA code[a]
(Fast Memory Used 1700K Bytes)

	Circular Crack Problem	End Effects Study Cylinder Lengths, mm			V-8 Cylinder	
		406[b]	686[c]	914[d]	Mesh No. 1	Mesh No. 2
Nodes	1286	1045	2573	2573	2328	3456
Elements	234	160	480	480	434	666
Equations (Degrees of Freedom)	3439	2726	7179	7179	6389	9603
Matrix Elements in millions (approx.)	1.5	0.64	3.2	3.2	3.1	6.2
Max. Half Bandwidth	962	509	900	900	1789	1543
Mean Half Bandwidth	436	231	943	943	485	645
Max. Block Size	67565	60127	39386	39386	44354	29226
Number of Blocks	29	11	82	82	71	216
CPU Time (Minutes) IBM 360/195	9	3.1	27	28	22	63
I/C (Thousands)[e]	28	46	50	175	105	492
Wall Clock Time (Minutes)[f]	37	90	175	250	125	585
Approximate Cost ($)	58	57	178	235[g]	165[g]	600[g]

[a]Object code obtained with the IBM FORTRAN H compiler. This version still had the sequential I/O routines.

[b]1500K region and 3K blocking factor for scratch units, unoptimized profile.

[c]One time step of the transient (also applies to 1219 mm cylinder).

[d]Three time steps of the transient.

[e]Depends upon blocking factor of the scratch units.

[f]In an "Multiprogramming with a Variable Number of Tasks" (MVT) environment, this can vary considerably for identical runs.

[g]Printed output to tape.

Conversion Factors for Units Used in This Report
(Reference: Metric Practice ASTM E380-76)

To Convert From		To	Multiply By
Stress/Pressure	$lbf \cdot in^{-2}$ (psi)	$kPa (kN \cdot m^{-2})$	6.894 757
Stress Intensity Factor	$ksi \cdot in^{-1/2}$	$MPa \cdot m^{1/2} (MN \cdot m^{-3/2})$	1.098 843
Coefficient of Heat Transfer	$Btu \cdot h^{-1} \cdot ft^{-2} \cdot °F^{-1}$	$W \cdot m^{-2} \cdot K^{-1}$	5.678 263
Heat Capacity	$Btu \cdot lb^{-1} \cdot °F^{-1}$	$kJ \cdot kg^{-1} \cdot K^{-1}$	4.186 800
Thermal Conductivity	$Btu \cdot h^{-1} \cdot ft^{-2} \cdot °F^{-1}$	$W \cdot m^{-1} \cdot K^{-1}$	1.730 735
Density	$lb \cdot ft^{-3}$	$kg \cdot m^{-3}$	16.01846

NUREG/CR-1499
ORNL/NUREG/CSD/TM-14
Distribution Category RF

INTERNAL DISTRIBUTION

1. B. R. Bass
2. B. R. Becker
3. S. E. Bolt
4. R. H. Bryan
5. J. W. Bryson
6. D. A. Canonico
7. H. P. Carter/A. A. Brooks/ CSD Library
8. S. J. Chang
9. R. D. Cheverton
10. J. M. Corum
11. W. B. Cottrell
12. J. R. Dougan
13. G. J. Farris
14. P. P. Holz
15-19. S. K. Iskander
20. J. G. Merkle
21. C. A. Mills
22. S. E. Moore
23. F. R. Mynatt
24. D. S. Napolitan
25. D. J. Naus
26. H. A. Pohto
27. J. L. Rich
28. G. C. Robinson
29. G. M. Slaughter
30. J. E. Smith
31. W. J. Stelzman
32. R. E. Textor
33. D. G. Thomas
34. H. E. Trammell
35. D. B. Trauger
36. G. D. Whitman
37. Patent Office
38. Central Research Library
39. Document Reference Section - Y-12
40-42. Laboratory Records Department
43. Laboratory Records (RC)
44. ORGDP CSD Library
45. ORGDP Library
46. ORGDP Plant Records

EXTERNAL DISTRIBUTION

47. Director, Division of Reactor Safety Research, Nuclear Regulatory Commission, Washington, DC 20555
48. Office of Assistant Manager for Energy Research and Development, Department of Energy, Oak Ridge Operations, Oak Ridge, TN 37830
49. C. Z. Serpan, Division of Reactor Safety Research, Mail Station 1130SS, U. S. Nuclear Regulatory Commission, Washington, DC 20555
50. M. Vagins, Division of Reactor Safety Research, Mail Station 1130SS, U. S. Nuclear Regulatory Commission, Washington, DC 20555
51-52. Technical Information Center, DOE
53-482. Given distribution as shown under category RF (10 copies — NTIS)